A SEARCH FOR EARTH-CROSSING ASTEROIDS

(NAGW-232)

SUPPLEMENT TO THE

SEMIANNUAL STATUS REPORT

L. G. TAFF, J. M. SORVARI, AND D. F. KOSTISHACK

LINCOLN LABORATORY, M. I. T.

LEXINGTON, MA 02173

COVERING JANUARY 1, 1983 TO JUNE 30, 1983

(Revised January 20, 1984)

CONTENTS

SUMMARY

M.I.T.'s Lincoln Laboratory has been supporting the Electronic Systems Division of the Air Force Systems Command in the development of the GEODSS (Ground-based Electro-Optical Deep Space Surveillance) program. This is a network of computer-controlled optical observations [40-inch (1-m) telescopes], equipped with large-format, low-light-level, television cameras of the intensified silicon-diode array type. It will replace the Baker-Nunn photographic camera system for artificial satellite tracking within the next few years. One element of this assistance has been the ab initio construction of a prototype observatory (the Experimental Test System or ETS) near Socorro, New Mexico. The discrimination of distant artificial satellites (angular speed $\approx$ 15" sec^{-1} from stars is performed in real time on the basis of the satellites' proper motion. It seemed logical to try the same technique to observe and search for minor planets (angular speed $\approx$ 0".01 sec^{-1}). This has necessitated some hardware modifications, which have been successfully performed, and asteroids can now be routinely observed and searched for at the ETS. The limiting magnitude is roughly B = $17^{m}.5$. The complete observing cycle, including the 2 - 3" measurement of position, requires about four minutes at present. The commonality of asteroids and artificial satellite observing, searching, data reduction, and orbital analysis is stressed. Improvements to the hardware and software as well as operational techniques are considered too.

This report represents a complete historical summary of Lincoln Laboratory's efforts in asteroid observing up to September, 1983.

I. OVERVIEW

The ETS exists to search for, detect, and observe artificial satellites by their reflected sunlight. The discrimination is facilitated by their large (∿15"/sec) intrinsic motions. Once found we record their positions for the initial generation of orbital element sets and for the refinement of existing orbital element sets. We also record various photometric data, both wide-band and multi-color, to detect any lightcurve variations and for classification purposes. In particular, the various periodicities in a satellite's motion relative to its center of mass (spin period, precession period, or nutation period), information concerning its size, shape and the nature of its surface, and the satellite's orientation are desired data. We also search for lost and unknown satellites in a variety of ways.

Each of the above types of operation and data acquisition and analysis have been, and continue to be, performed for asteroids (or minor planets). The first searches were conducted in 1800; over 2900 asteroids are now permanently catalogued and several thousand new objects are discovered yearly. That the relationship between artificial satellites and minor planets goes fairly deep should not be surprising. Asteroids are natural satellites of the Sun shining by reflected sunlight. They come in a large variety of sizes, shapes, surface reflectivities, spin periods, orientations, etc. They and comets span the limits of orbital element space much as deep space artificial satellites do. This commonality of aspects implies a commonality of observing techniques, analysis techniques, and the fruitful cross-fertilization of the two fields.

So far this flow has been mostly one way - from minor planet work to artificial satellite work. We have now extended minor planet research, especially with regard to initial orbit generation and search techniques, thus evening things up a bit. Because we are extending artificial satellite work at the same time and in the same areas, NASA has benefited by not having to pay for this work. Moreover, because we've had Air Force funding for our observatory in the past, NASA has never been asked to pay for telescope time.

There is another significant advantage in the case of the ETS for asteroid searches. Since no other observatory is as well equipped as the ETS is for performing the real time detection and discrimination of minor planets, or for obtaining their positions in real time, the telescope time is efficiently used. The other point is that no other observatory is capable of performing a real time search for asteroids. Here, especially for the increasingly important Earth-approaching objects, the ETS can play a unique role. To understand the latter point in more detail consider photographic asteroid searches. A 6° x 6° photographic plate secured at New Moon in the direction of opposition could easily contain 200 - 300 main belt minor planet trails. (The generic main belt asteroid is in a circular orbit that lies in the ecliptic 2.7 A.U. from the Sun.) One must search the developed plate, with a microscope, looking for the trails indicative of an asteroid. This requires about 30 hours. Then, after the trails are marked, one must find reference stars (from either the SAOC or the AGK3). Next the plate must be measured, both trails and stars, and the measurements reduced. This requires another 30 hours. Thus, if it requires 60 hours for 300 asteroids the average service time is 12 minutes/minor planet and the search rate is at most 1.2 square

degrees/hour. In contrast, at the ETS, the service time is 3-4 minutes/minor planet and the search rates vary from about 10 to about 90 square degrees/hour as we go from the zoom Cassegrain configuration to the non-zoom prime focus configuration. The photographic position will be good to 1" while ours is 2-3". This can be improved by repetition.

In practice the photographic search rate for fast moving objects can fall in our midrange. The reason is simple--fast moving (say Earth-approaching) minor planets will leave a relatively long trail on a photographic plate (compared to a mainbelt asteroid's trail length for a fixed exposure time). Hence, if these plates are developed and inspected immediately after exposure, but only exceptionally lengthy trails are looked for, the fast moving minor planet search rate can be 72 square degrees/hour (say two 6° x 6° plates with 20 minutes for exposure, 5 minutes for developing, and 5 minutes for a rapid scan).

A. Historical Background

Three trips were made to the ETS by L. G. Taff, John Sorvari, and the requisite equipment for asteroid observing in November 1979, January 1980, and May 1980. The purpose of the first trip was to make sure that we (Dave Beatty, John Sorvari, and L. G. Taff) knew what we were doing and that we had the correct equipment. The purpose of the second trip was to pin down the operational limiting magnitude. Our own multicolor photometry indicated $B = 17^{m}.5$ in the zoomed Cassegrain configuration. The purpose of the third trip was to refine our technique and perform some observations specifically for Brian Marsden (Director of the Minor Planet Center). Hence, as far as we were concerned, our exploratory operational phase was completed and the design and implementation of the search should commence. A proposal was

submitted to NASA to partially fund Earth-approaching asteroid searches in July of 1980. A revised version was funded in June of 1981. We asked for and received a no-cost extension in June of 1982. In February of 1982 Daniel F. Kostishack and L. G. Taff submitted a proposal for the continuation and upgrading of our searches (via a CCD camera). This was approved and extended through March 31, 1984. As will be discussed below we feel that we are at our maximum performance and would like to continue asteroid searches at this level for the next 3-5 years.

II. HARDWARE AND OPERATIONS

A. The Observatory

The ETS is a duplex observatory. One-half of it consists of two telescopes comounted on an equatorial mount. The main telescope is a 31-inch (79-cm), f/5, f/2.8 Ritchey-Chretien unit, providing nominal 1°2 and 2° (6".5 pixel size) fields of view on a flat 80-mm face plate located in the focal plane. The auxiliary telescope is a 14-inch (36-cm) f/1.7 folded Schmidt unit, providing a nominal 7° field of view on an 80-mm faceplate. Operations are controlled from a console in a separate building. The main computer is a MODCOMP IV-25 which provides 256 kilobytes of core and includes 50 megabytes of disk-memory. The satellite file (containing ≃ 500 "deep-space" element sets) and the Smithsonian Astrophysical Observatory Star Catalog are the major files to which the computer has fast access.

After a series of field tests in 1972, it was decided that low-light-level, beam-scanned, television camera tubes of the intensified silicon-diode array type, generically called EBSICONs, possessed the necessary detection capability for real-time work. These tests also indicated the usefulness of an external, single-stage, image-converter tube coupled to the EBSICON. Another important advantage was realized by the use of a 2:1 demagnifying image converter. Finally, the increased prescan electron gain (≃ 25) provided by the external converter allowed the use of uncooled, 7.5 MHz video preamplifiers under the darkest skies at ETS. In addition, the camera target is etched with a fiducial mark to facilitate repeated, accurate positioning of the telescope. More detailed descriptions of the observatory and its hardware can be found in Weber (1979a,b).

B. Hardware Design Considerations

To discriminate minor planets from stars by their proper motions the basic electronic hardware associated with the video imaging system is the same as for an artificial satellite moving target indicator. The design of such a system is schematically shown in Fig. 1. As with its radar counterpart, the essential features are a storage medium, a delay line, and the capability to subtract the current signal from the stored one. Detection is performed after the differenced image is obtained. For minor planets we serve as the detector--hence our system is not automated in this respect.

The purpose of the delay line is to allow for a sufficiently long time interval during which the minor planet can traverse several (clearly at least 2) resolution elements of the camera target. For the artificial satellites within ETS coverage a typical delay time is ≈0.5s (e.g., resel size ≈3".5, angular speed ≈15"/sec.) The extremes would be $0^{s}.02$ and $1^{s}.5$. Since a typical asteroidal geocentric angular speed is $\lesssim$50"/hr the appropriate delay interval is in excess of 9 minutes. Hence, were this mode of operation followed, neither efficiently conducted searches nor efficiently performed positional measurements would be possible. Clearly it's much more effective to use the delay time to look for other minor planets and this implies a "delay line" capable of storing as many video frames as we can acquire during the $\lesssim$9 minute interval. Further, since 3-5 resels are much better than two and many asteroids move even slower than 50"/hr the "delay line's" storage capability should be at least 50 frames. Moreover it would be extremely convenient to be able to access any of these frames at random. Therefore, the simple delay line of Fig. 1 will be replaced by a random access multiple frame video storage device.

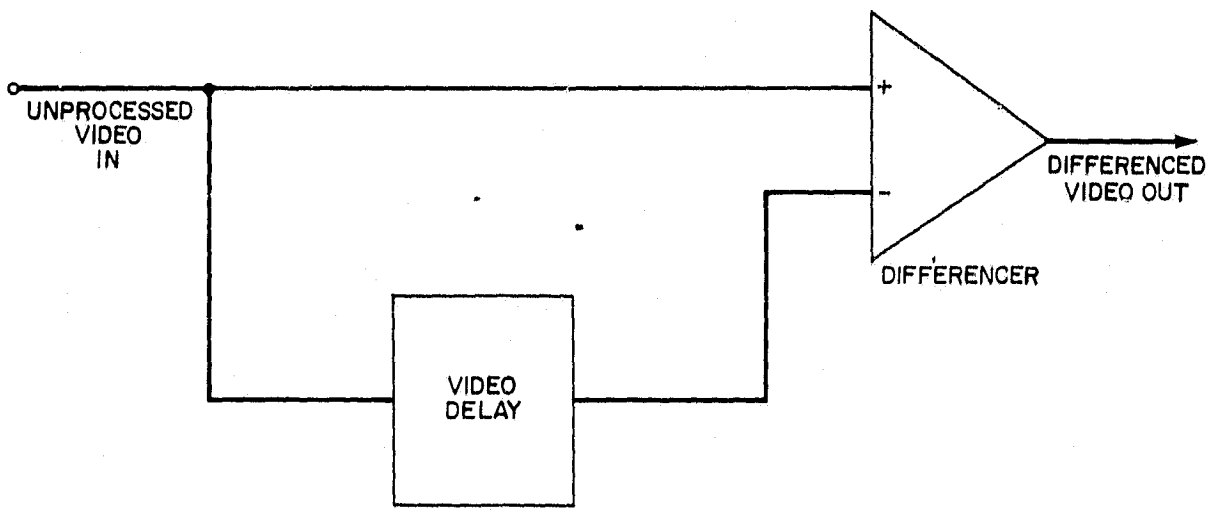

Figure 1. Basic Moving Target Indicator system block diagram.

Given the (originally) tentative nature of this type of observing, the availability of an analog disk storage device within Lincoln, and the quality of our video tape recorders, we decided that the special purchase of neither a digital disk storage device nor a modern studio grade video tape recorder could be justified. However, as we have inaugurated a minor planet search and observing program we have upgraded out video tape recorder(s), acquired a digital disk video storage system, and made other generalized improvements within the ETS's video system. This equipment was justified because of the commonality between minor planet work and artificial satellite work and paid for by the U.S. Air Force.

C. The Prototype System

A simplified block diagram of the moving target indicator system we've devised is shown in Fig. 2. The delay line of Fig. 1 has been replaced by two elements, an analog disk video storage unit and a video integration/storage device. The latter is used to increase the unprocessed video signal level above the minimum signal-to-noise ratio necessary to recover it from the storage medium. This increases our limiting magnitude with a negligible loss of efficiency. There are two basic types of such devices--analog and digital.

An analog storage tube scan converter has been used at the ETS for several years. Because of imperfections in the silicon target storage element, principally blemishes and variable response across the target face, the complete cancellation of successive video frames is difficult to accomplish.

Digital image processing and storage systems are more attractive than analog ones because they don't suffer from these defects and they are programmable. The one we've used (again principally because of immediate availability

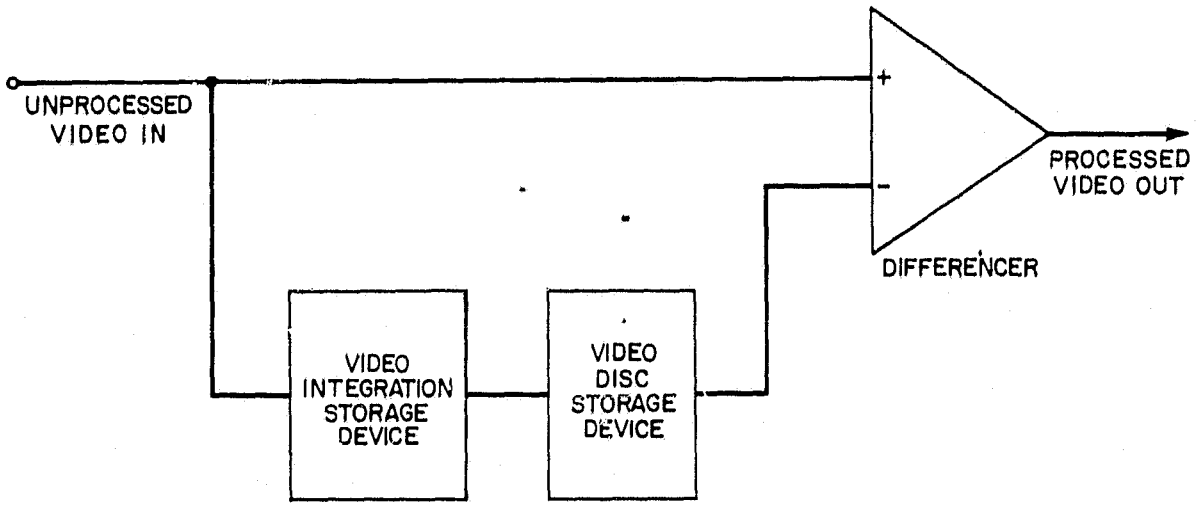

Figure 2. Simplified Minor Planet MTI block diagram.

within Lincoln) is a Quantex Corporation DS-20 (Fig. 3). It stores 12 bits/resel of amplitude information and has a 512 x 512 resel format. Among other tasks it can be programmed to difference frames, store them or recover them. Coupled with this is our analog disk video storage medium, an Echo Science Company EFS-1A Discassette Frame-store color video recorder. This is also shown in Fig. 3. The third unit in Fig. 3 was used to synchronize the video signals.

The video differencing itself could be accomplished by a simple high frequency operational amplifier--if all system delays and signal level shifts could be neutralized. In practice this is extremely difficult to do. Hence the following alternative was devised: The Quantex DS-20 digital video processor is switched from its recording function when the reference (i.e. original) frame is stored to that of a differencer between the Echo EFS-1A video disk storage unit and the comparison (i.e. the subsequent) frame. This is illustrated in Fig. 4 which is a full block diagram of the prototype minor planet moving target indicator.

Additional equipment to provide discrimination includes video distribution amplifiers for video isolation within the processing equipment and the appropriate coaxial switches. Table I contains a complete list of all of the discrimination hardware. As mentioned above one of us serves as the detection instrument and our operating characteristics are discussed below.

D. General Method of Operation

With reference to Fig. 4, during the recording phase of the operations video switches 1 and 2 are in position #1. The telescope is pointed, set into sidereal drive, and the digital storage and integration unit (the DS-20) activated. It integrates until the saturation level is reached within a resel

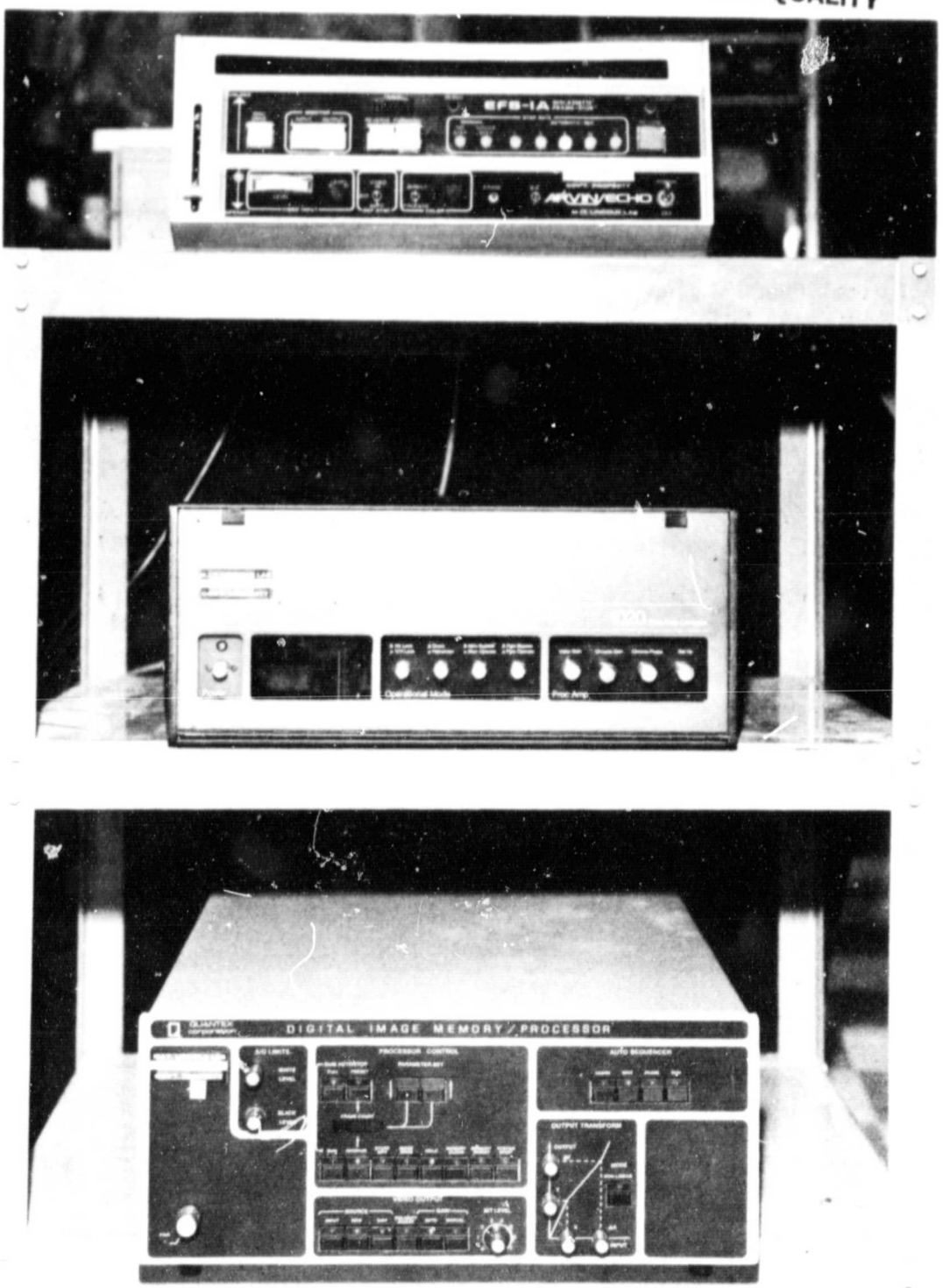

Figure 3. The Minor Planet MTI hardware (original). The Arvin Echo EFS-1A is at the top, the Quantex DS-20 is at the bottom. The time based corrector (middle) is no longer used.

TABLE I

EQUIPMENT LIST

Disk Storage Unit	ARVIN Echo Model EFS-1A
Digital Storage and Integration Unit	Quantex Model DS-20
Time Base Corrector	Microtime Model 1020
2 ea. VDA (Video Distribution Amplifier)	Telemation Model TVA-525
2 ea. Video Switch	Matrix Systems Corp. 7104

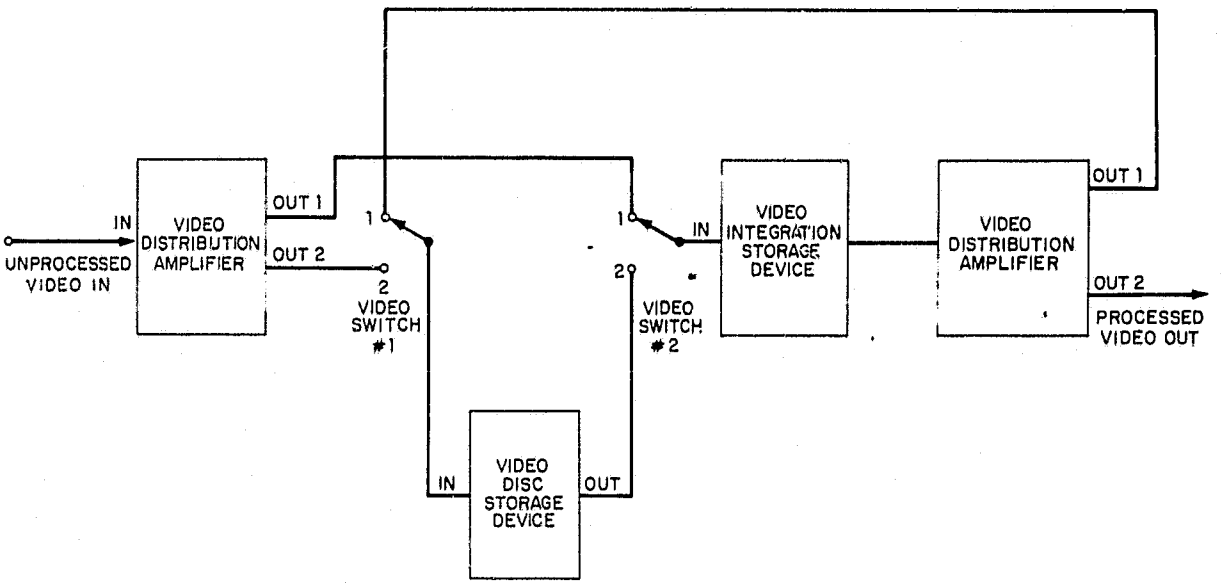

Figure 4. Full block diagram of the original asteroid MTI with the video switches in the Record positions.

(typically $\sim 2^s$). This integrated image is stored, as a single frame, in the analog disk video storage device (the EFS-1A). The telescope is moved to the next position and this process repeated. This continues until the appropriate time interval ($\sim 30^m$) has elapsed and we then return to the original field. We now recover the appropriate frame of stored data and place video switches 1 and 2 into the #2 position. We also reprogram the DS-20 for the differencing mode. The first step is to repeatedly sum the reference frame in the DS-20 until saturation occurs. This is equivalent to signal averaging and is necessary if the full recovery of low signal-to-noise (e.g., faint) images is to occur. It also reduces the noise levels inherent in the video recovery process within the EFS-1A itself. Now live video (the comparison field) is fed to the DS-20 and the differencing performed. Constant objects are cancelled at this stage appearing only at the background level. An object that has moved appears twice, once as a negative (or dark) image from the reference frame and once as a positive (or light) image from the comparison frame. Figures 5-9 illustrate this.

These pictures were made by overprocessing some video tape recordings (to increase the contrast), playing the result through a television monitor, and then photographing the television monitor screen. The original video tapes were made at the instant of detection (for purposes other than the generation of Figs. 5-9) and more than anything else they illustrate that for asteroids this bright ($\sim 15^m$) discrimination is instantaneous. The image at the telescope console that the (human) detector sees is much better than Figs. 5-9 would indicate.

Figure 5. Detection of 85L Newcombia (nearest center, lower right quadrant) and another main belt asteroid (lower right quadrant).

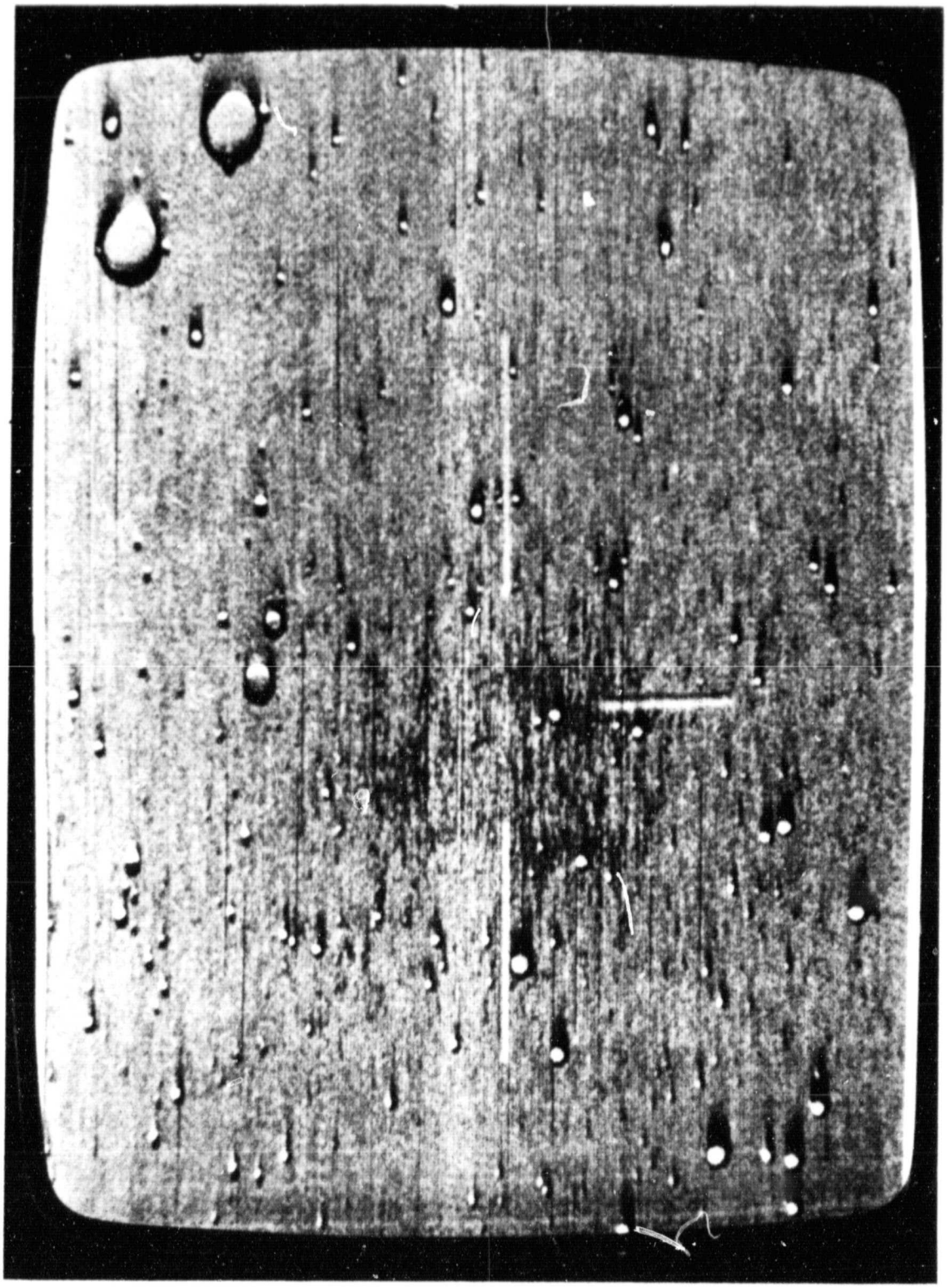

Figure 6. Detection of 265 Anna (lower right quadrant). Note that the white dot is below and to the right of the corresponding black dot.

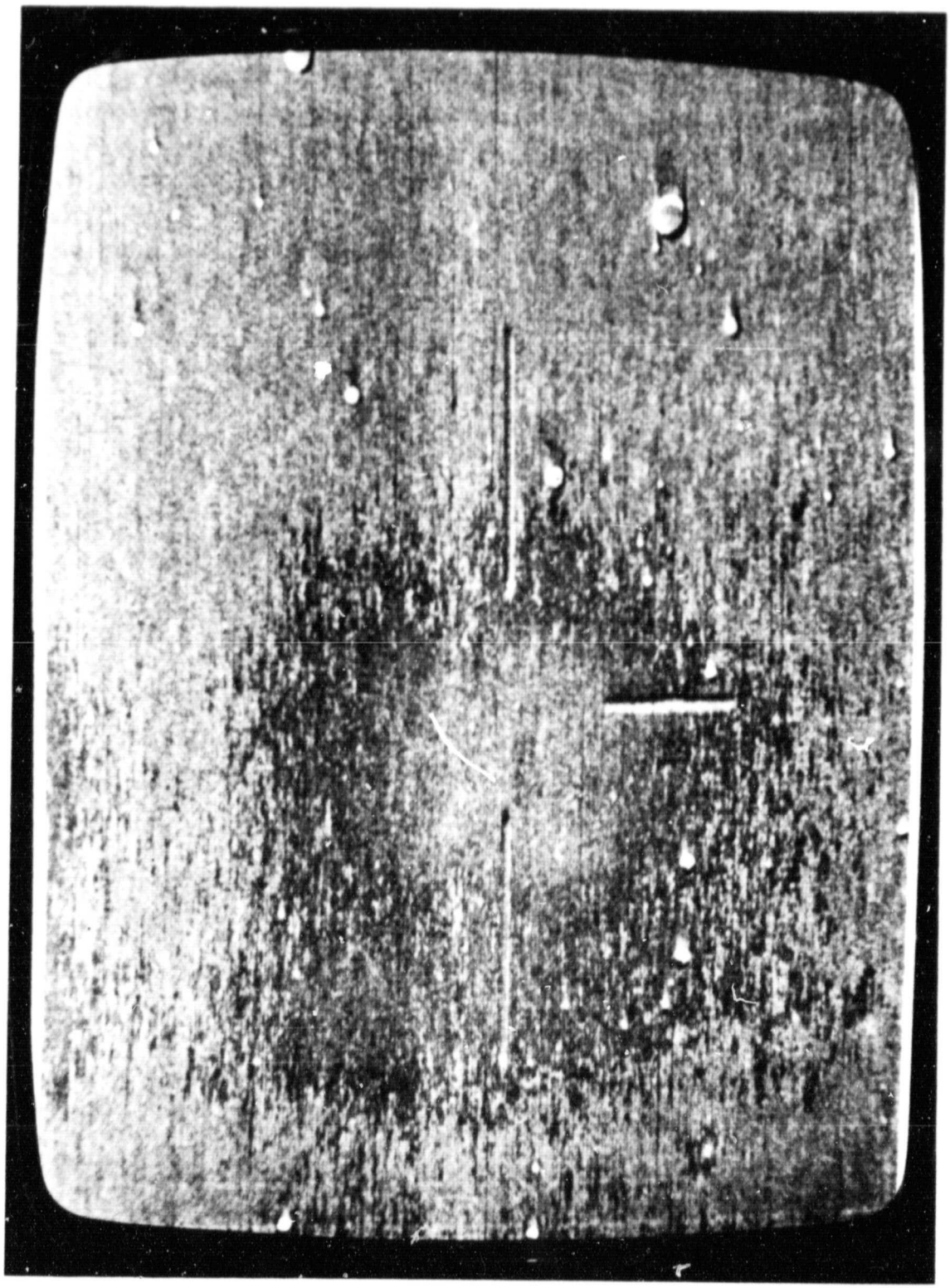

Figure 7. Detection of 1391 Corelia.

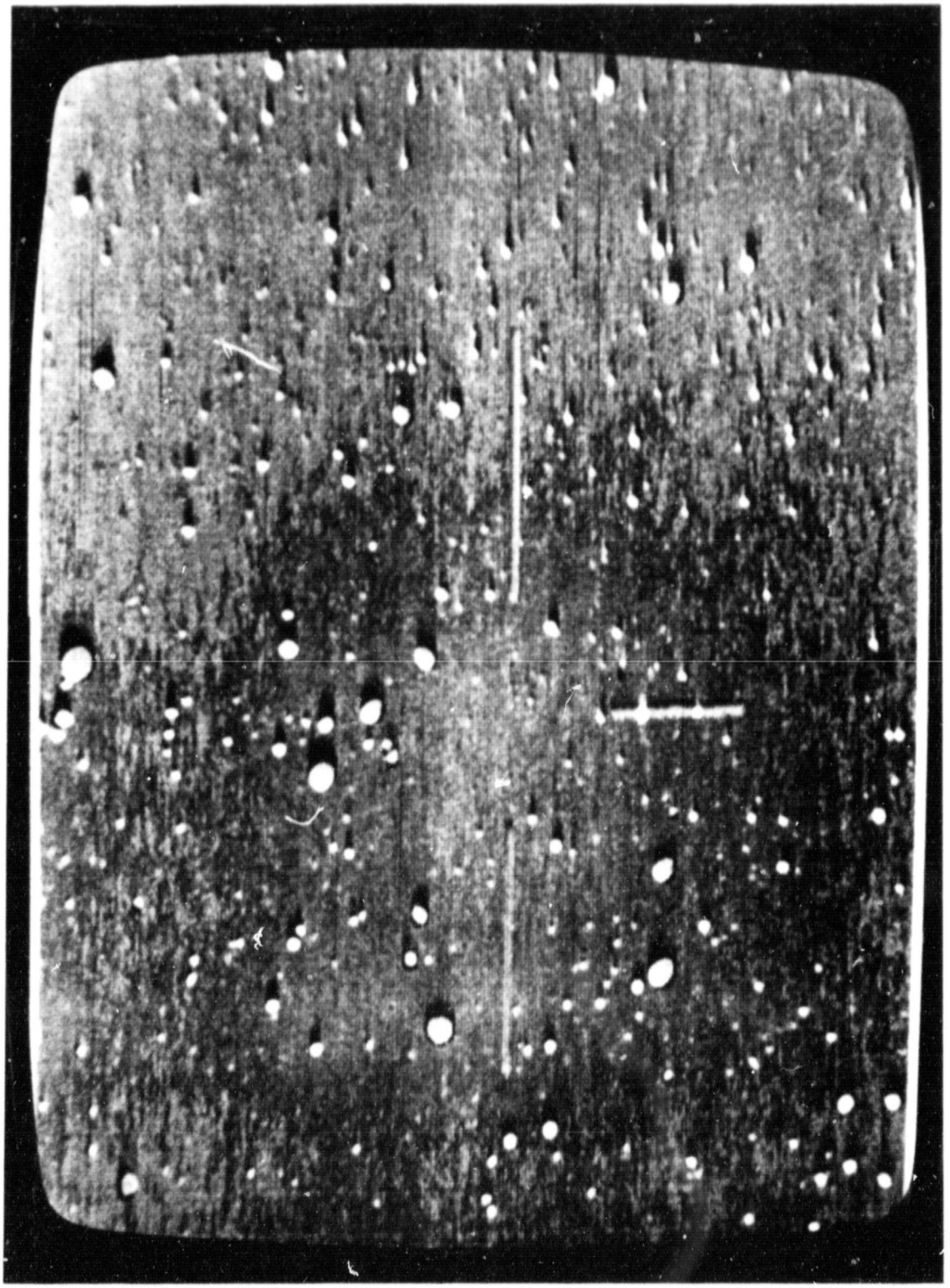

Figure 8. Detection of the Trojan asteroid 1867 Deiphobus.

Figure 9. Detection of 1684 = 1951 QE.

With a preprogrammed set of coordinates the sky can be covered almost as fast as we can start, move, and stop the telescope. In practice, including image quality checks, etc., we spend 10-15 seconds per field acquiring the reference image. The preprogrammed search patterns we most frequently use are box scans along or perpendicular to the ecliptic and spiral scans starting from opposition. In all cases the field-of-view, overlap, time spent per field, total area to be searched, etc., are adjustable parameters which are entered at the initiation of a search. Repetition of the last search pattern is initiated by a single button push. The actual search rate depends on the telescope/camera configuration of which there are three--prime focus non-zoom (largest pixels, brightest), Cassegrain non-zoom, and Cassegrain zoom (smallest pixels, deepest). Since all of our operations are essentially constant in time, it is only the ratio of pixel size areas that is changing the search rate in a 1:3:9 ratio.

E. Current Observing Procedures

Searches for Earth-approaching asteroids have been conducted during all but the Summer new moons for the last three years. The best times of year (historically) for such searches are the Fall and early Winter new moons. Within a new moon period, depending upon the weather, our searches may start as early as two days after third quarter moon or extend as late as two days before the first quarter moon.

We generally search around the opposition point (e.g., that point on the celestial sphere with coordinates $\alpha_\odot + 12^h$, $-\delta_\odot$ where $\alpha_\odot$ is the right ascension of the Sun and $\delta_\odot$ is the declination of the Sun) in rectangular

boxes. Each of these boxes consists of 49 fields of view. The pattern is shown in Fig. 10. Each of the smaller boxes is 0°.84 x 0°.66 so the total area covered at the equator is 27.2 square degrees. An area such as this is covered twice - once in the reference frame storage mode and once in the comparison frame mode. The first phase lasts about 15 minutes (including a 6 minute wait for an asteroid to cross at least one resel at the minimum interesting angular speed of 1"/min - about twice the typical main-belt asteroid speed). It requires 9 minutes to successively accelerate the telescope, move it, decelerate the telescope (about 6 seconds per sequence at present), and then store the resulting new field of view. The second phase typically requires 30-50 minutes. It depends on the weather, the hour angle of the search area (because distortions due to interaction with the Earth's magnetic field increase away from the celestial meridian), and the number of objects found.

F. The New Hardware Configuration

The live signal from the television camera is signal averaged (16 frames worth) in a Quantex Corp. model DS-20 digital video integration/storage device. In the reference frame phase the result of this operation is stored in an ADDA Corp. model ESP-100B electronic still processor. This device has 200 randomly accessible frame storage locations and two output channels. In the comparison frame phase the signal averaged comparison frame is passed through the other channel of the ADDA to eliminate systematic effects due to different handling of the image. Note that since we return to the last boxes of a scan with a sufficient time lapse for a main-belt asteroid to be found we will find some. This is rewarding, proves (to ourselves) that all is well with our equipment and techniques, and contributes to general minor planet research.

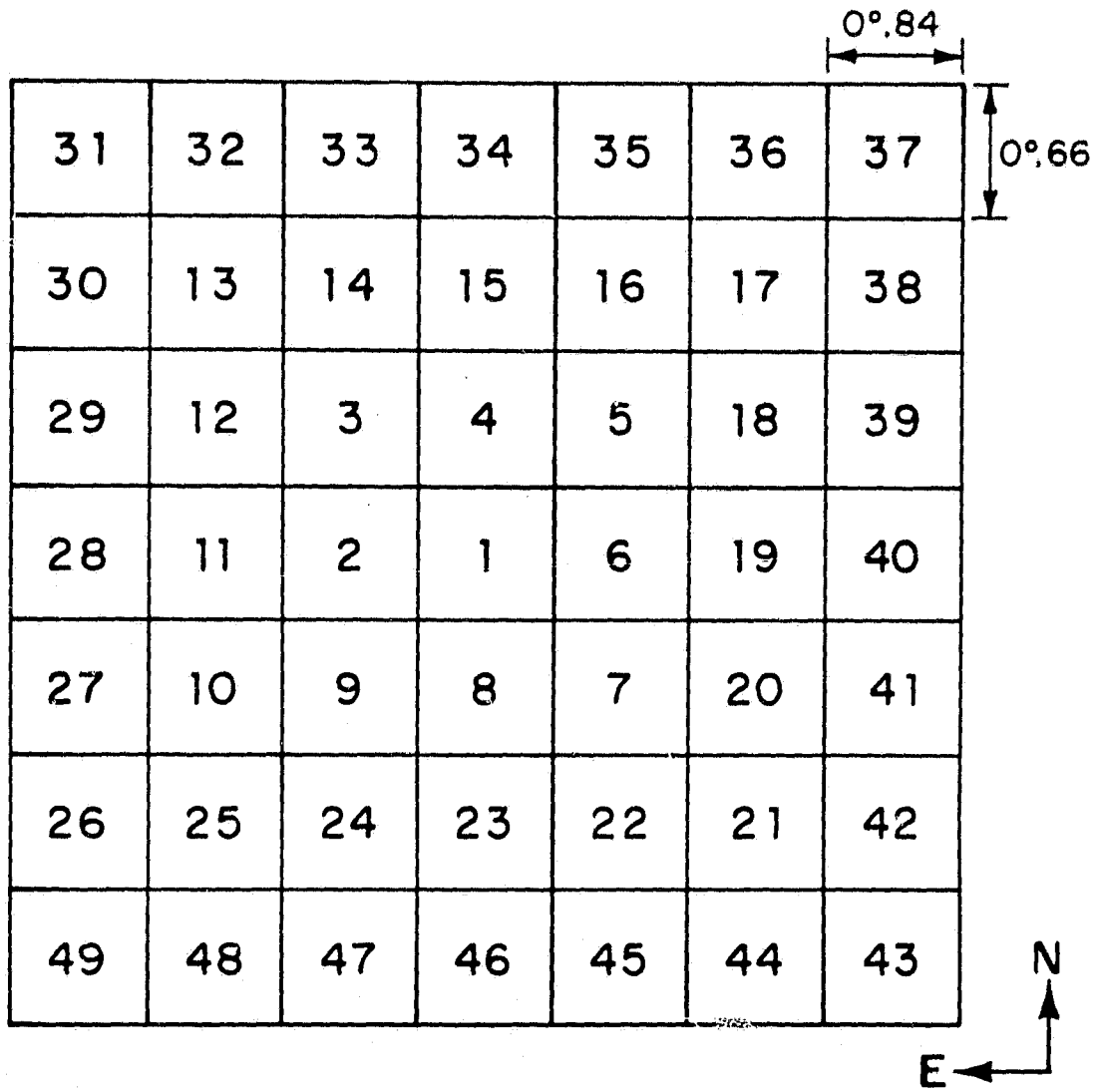

Figure 10. Search pattern of spiral scans. They may enclose 1, 9, 25, 49, 81, etc. boxes.

During the second phase of the procedure the observer is looking at the difference between the live image (the comparison frame) and the stored image (the reference frame) from the first phase. Objects which haven't moved cancel, objects that have moved an appropriate amount show up as two uncancelled dots - one black and one white. Artificial satellites, which all move too fast, leave only a single dot. Photographs of what we see at the telescope console usually raise more questions to the uninitiated than they answer, but a photograph of the screen with 927 Ratisbona at B ≈ $14^{m}.3$ on it is shown in Fig. 11. The time interval was much larger than is usual for illustrative purposes and there is only one asteroid in the picture.

The search rate is between 25 and 35 square degrees per hour depending upon the rapidity of the comparison phase. The limiting magnitude on a good dark night is about B = $17^{m}.5$. There are no external false alarms. The internal false alarm rate (e.g., requiring a minute or two of telescope time to definitively resolve) is about 1-3 per 49 box scan. We operate at the Cassegrain focus and not in the electronic zoom mode. Also, the number of boxes in a scan is variable as is the box-to-box overlap, timing, etc.

The last step, in the comparison frame phase, is to recall the appropriate storage location within the ADDA as the comparison frame is being processed by the ADDA, and then pass both of these through an analog operational amplifier for differencing. The result is then displayed for the operator (cf. Fig. 11). Figure 12 is a schematic block diagram of the current system. D. E. Beatty has been responsible for all of our hardware configurations.

Figure 11. Asteroid 927 Ratisbona at B≈14^{m}.3.

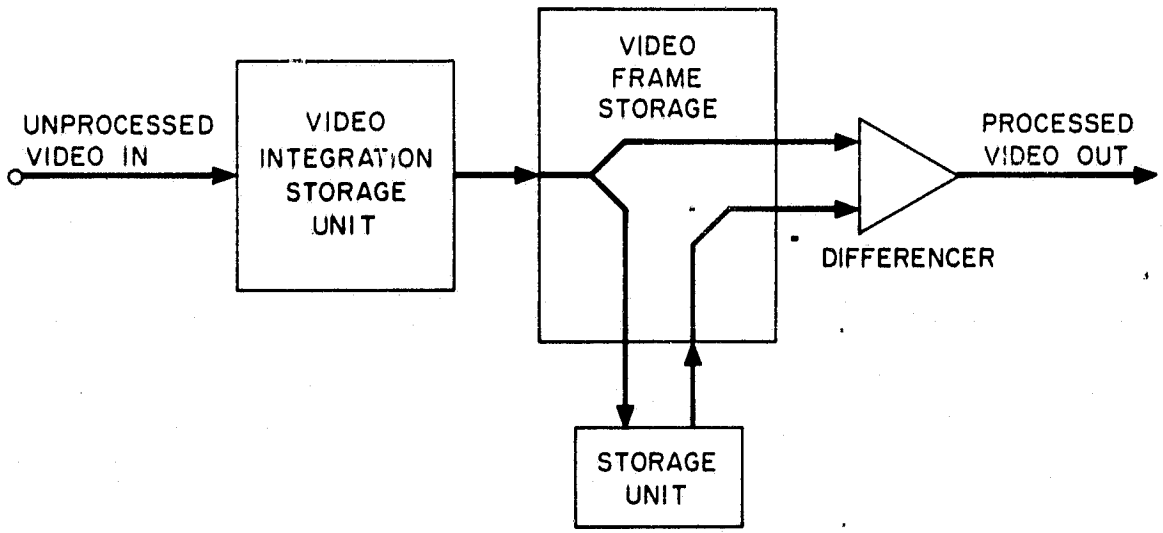

Figure 12. Block diagram of current minor planet moving target indicator.

The use of a CCD camera instead of an Ebsicon camera is transparent to the observer. There will be different search rates and limiting magnitudes for the non-zoom Cassegrain configuration and for the zoomed prime focus configuration (both faster and deeper).

G. Limiting Magnitude

In astronomical photography the concept of a limiting magnitude is well defined and depends solely on the physical properties of the system. Depending upon other variables, the limiting magnitude may be achieved in a few minutes or many hours exposure. This sort of limiting magnitude is not particularly applicable to the case at hand. The point of the experiments we conducted was to find objects of unknown location by searching for them. Increasing the exposure thus has a strongly negative effect in that it sharply decreases the area which can be searched. Since the search is conducted in real time it is also necessary to include extra time for an observer to detect any object which has been discriminated by the hardware. Clearly the desired goal is to maximize the probability of finding a suitable object. The brighter the object sought the more quickly it can be found and the greater the searched area can be. The fainter the object sought the more of them there will be. We may instead think of a practical limiting magnitude. Our experience has been that down to some level of brightness any candidate may be found within about twenty-thirty seconds and that very few (presumably slightly fainter) are found by extending the examination time to several minutes. In this regard it is possible to draw on our extensive experience with satellite detections. Changing the operational parameters of the video system makes it easier to find marginal detections, but

to a large extent this is merely a trade between exposure time and examination time to no overall benefit.

Based on the preceding considerations, we have decided to accept as a practical limiting magnitude the brightness of the faintest objects which are found within 30 seconds with the "standard" hardware configuration described above. It is to be expected that slowing the search would allow detection of a few tenths of a magnitude fainter, but that this could not be justified unless there were reason to believe that the distribution of minor planets with apparent magnitude was much steeper than anticipated (e.g., exponential) or that the appropriate search region was considerably smaller than we currently feel it is.

The night on which the brightness measurements were made was of marginal quality - a space of a few hours between two completely clouded periods. The period of measurement seemed to be fairly uniform until the clouds returned. This can be quantified by the internal consistency of multiple measurements which showed the measurement error to be only slightly larger than could be expected from the counting statistics alone. It is this measurement error which is quoted below. An additional error source - error in the correction for extinction - is expected to be negligible compared to the measurement error for threshold objects. Measurements of the two faintest asteroids found gave values of $m_x = 16^m.4 \pm 0^m.3$ and $16^m.6 \pm 0^m.2$. The x-subscript denotes measurement through a filter commonly used at the ETS which has a central wavelength of 0.67μ. The x-filter magnitude is defined so that $m_v = m_x$ for solar colored objects. Thus we estimate the limiting V-magnitude at $m = 16^m.7 \pm 0^m.2$ or, as is commonly quoted, a limiting B-magnitude of $B = 17^m.5 \pm 0^m.2$.

H. The CCD Camera Upgrade

For the last six years a CCD technology development program has been in progress at Lincoln Laboratory. Both the Space Surveillance and Microelectronics Groups have pursued the development of CCD imagers and related system concepts. The objectives of this work have been improved performance and reliability for the U. S. Air Force's Ground-based Electro-Optical Deep Space Surveillance network (GEODSS). In particular, a deeper limiting magnitude and higher search rates than are obtainable with Ebsicon cameras were desired. For this purpose a low-light level, large format (100 x 400 pixels), ultra-low noise, low dark current, and good quantum efficiency CCD imaging device was built at Lincoln. Along with this work was the design of focal plane structures, search strategies, signal detection and discrimination processing, etc., as reported in Kostishack, Burke, and Mayer 1980. Both laboratory and field tests at the observatory (the Experimental Test System or ETS) were conducted with results reported in Kostishack et. al. 1980. Additional CCD work has included the development of a 30 x 30 pixel CCD photometer and closed loop automatic tracking sensor; a CCD camera for the daylight tracking of artificial satellites; a panoramic CCD sky monitor to use in real-time scheduling in partly cloudy weather; and most importantly, the design and building of a CCD camera to be used on a retrofit basis at the deployed GEODSS sites. The deployment of these cameras is expected within two years.

The development of the retrofit camera, while not ideal for minor planet work, addresses many of the same questions. Table II summarizes the primary reasons for preferring a CCD camera over an Ebsicon camera. Of additional

TABLE II

CCD VERSUS EBSICON SENSORS

IMPROVED PERFORMANCE FOR SATELLITE SURVEILLANCE AND ASTEROID SEARCH

- INCREASED ELECTRO-OPTICAL AND DETECTION SYSTEM SENSITIVITY
- INCREASED SCAN COVERAGE OR SEARCH RATE
- IMPROVED PRECISION POSITION CALIBRATION AND MEASUREMENT

PROJECTED GREATER AVAILABILITY OF CCD's BECAUSE OF COMMERCIAL INTEREST

CCD TECHNOLOGY

- HIGH QUANTUM EFFICIENCY
- SMALL SIZE, LARGE NUMBER OF PIXELS
- CONSTANT, ACCURATE SENSOR PIXEL GEOMETRY
- STABLE, REPRODUCIBLE, RELIABLE CHARACTERISTICS

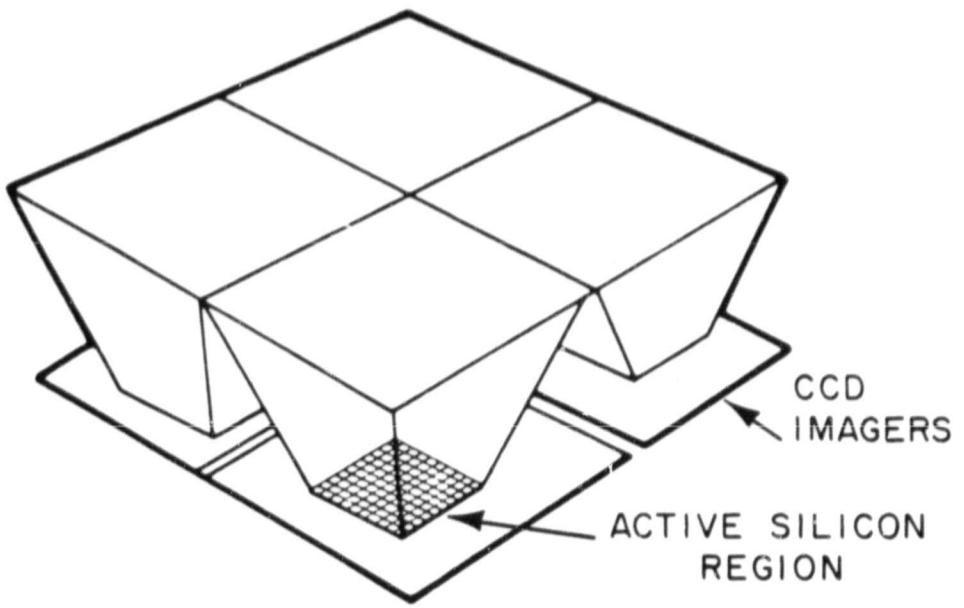

- PERMITS USE OF EXISTING COMMERCIAL CCD IMAGERS
- CONTROL OF PIXEL SIZE
- FULL FOCAL PLANE COVERAGE

Figure 13. Fiber optics focal plane reducer.

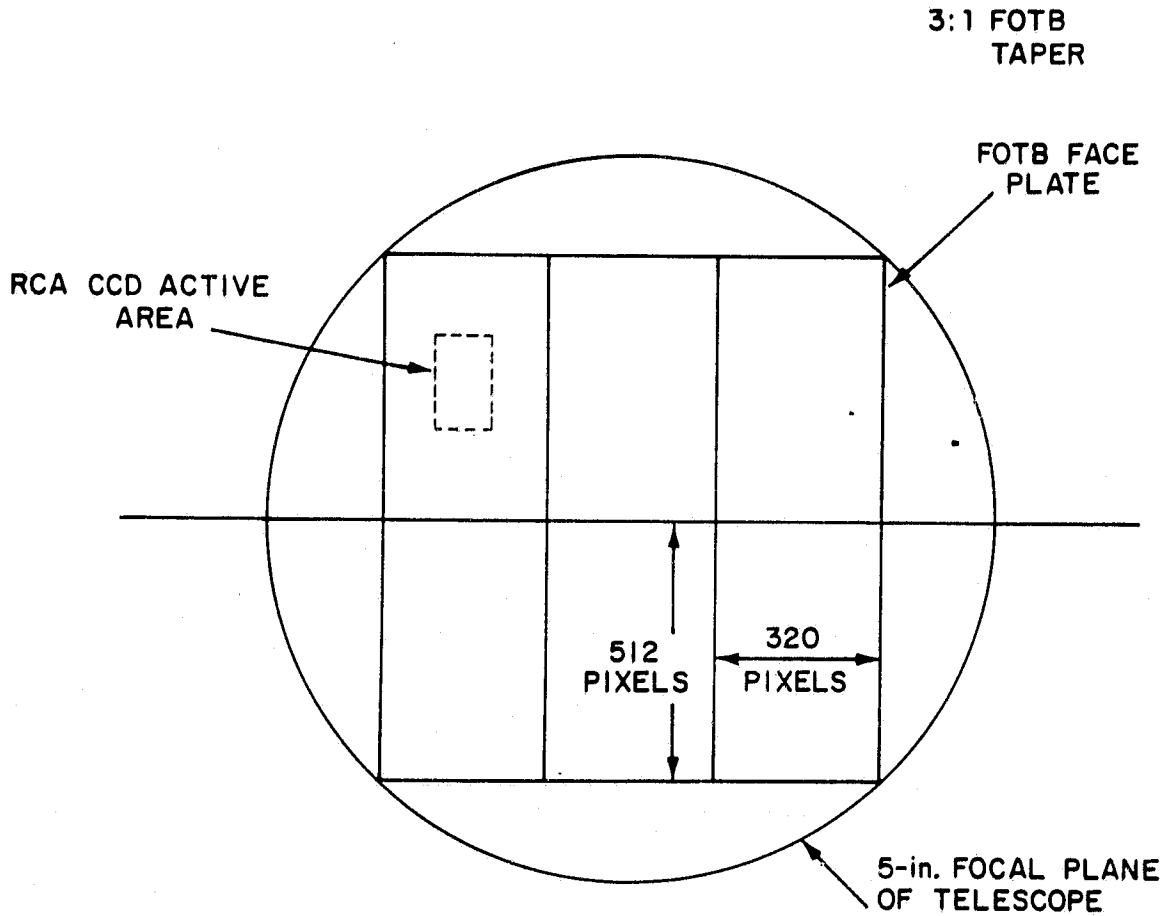

Figure 14. 6-CCD/FOTB camera focal plane geometry.

CHARACTERISTICS	REQUIRED	RCA-SID
TRANSFER EFFICIENCY	0.9999	0.99997
DEVICE NOISE	$35e^-$	$70e^-$
DARK CURRENT	5nA	5nA
DYNAMIC RANGE	10^4	5×10^3

FEATURES MEASURED TO BE ACCEPTABLE

- BLOOMING CONTROL
- OPERATION COOLED TO -50°C
- OPERATION AT LOWER CLOCK RATES
- RESPONSE UNIFORMITY
- DEFECTIVE PIXEL COUNT
- SMALL SIGNAL TRANSFER EFFICIENCY

QUANTUM EFFICIENCY

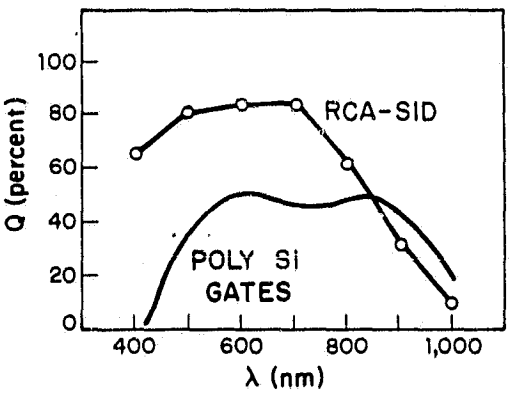

Figure 15. RCA SID-53612 CCD imager characteristics.

importance for asteroid work is the geometrically stable format of the CCD which allows for better signal processing and longer integration times.

Further relevant properties of this camera and the associated focal plane structure are the use of the highest performance commercially available CCD imaging devices and the use of a fiber optics tapered bundle (see Fig. 13) structure. This allows complete, leakproof coverage of the focal plane while simultaneously permitting a change in effective pixel size. As most commercially available CCD devices have too small a pixel size, the exploitation of taper ratios in excess of 3:1 is extremely advantageous. The maximum usable focal plane of the 31 inch telescope at the ETS is 125mm. The Ebsicons only use 80mm. Thus, the search rate could be 2.5 times as fast if the full focal plane could be utilized. This could be done by using a fiber optics tapered bundle structure. In particular, with a 3:1 taper ratio and the 30μ pixel RCA SID device, a total of 6 CCD chips would cover the focal plane as shown in Fig. 14. These chips (see Fig. 15) are thinned, back-illuminated, low-light-level, with a 512 x 320 pixel format. They are also the highest performance, commercially available chips.

If some modest improvements in the computer control of the telescope are made and simultaneously the actual search procedure is tightened, such a design would yield a 600 square degree per hour scan coverage rate. The limiting magnitude would be $V = 17^{m}.7$ ($B = 18^{m}.5$) against a $20^{m}.5$ per arc second squared sky background. Considerable additional video processing and storage equipment would also be necessary (Fig. 16) as well as 3 observers. It is estimated that it would require 2 years to put this package together. Most of the estimated $500,000 expense is in manpower and special purpose (e.g., asteroid only) video equipment.

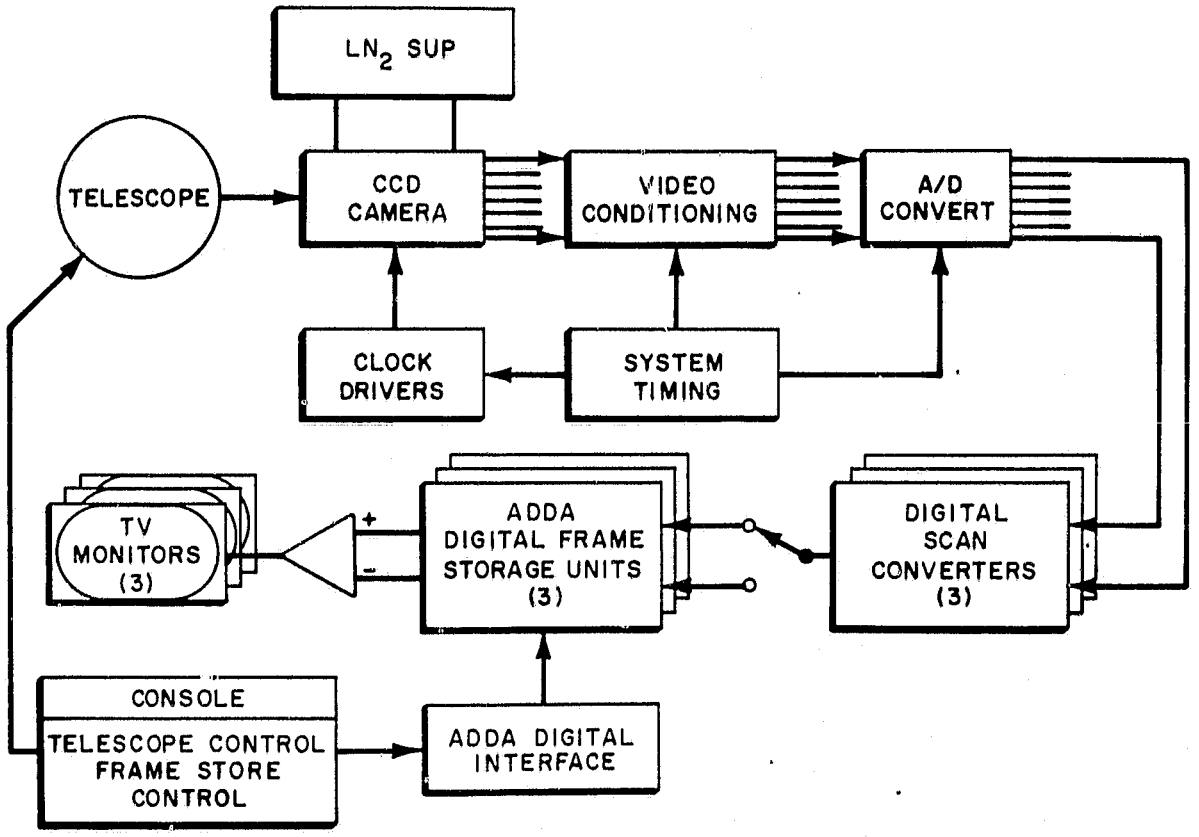

Figure 16. Six-element CCD camera system.

Table III

Asteroid Search System Candidate Designs

For GEODSS-ETS

- PERFORMANCE COMPARISON -

	SENS (m_v)	SEARCH RATE (deg^2/hr)
PRESENT EBSICON SYSTEM	16.7	27
6-CCD/FOTB CAMERA SYSTEM	17.7	600
2-CCD/FOTB CAMERA SYSTEM	17.7	200

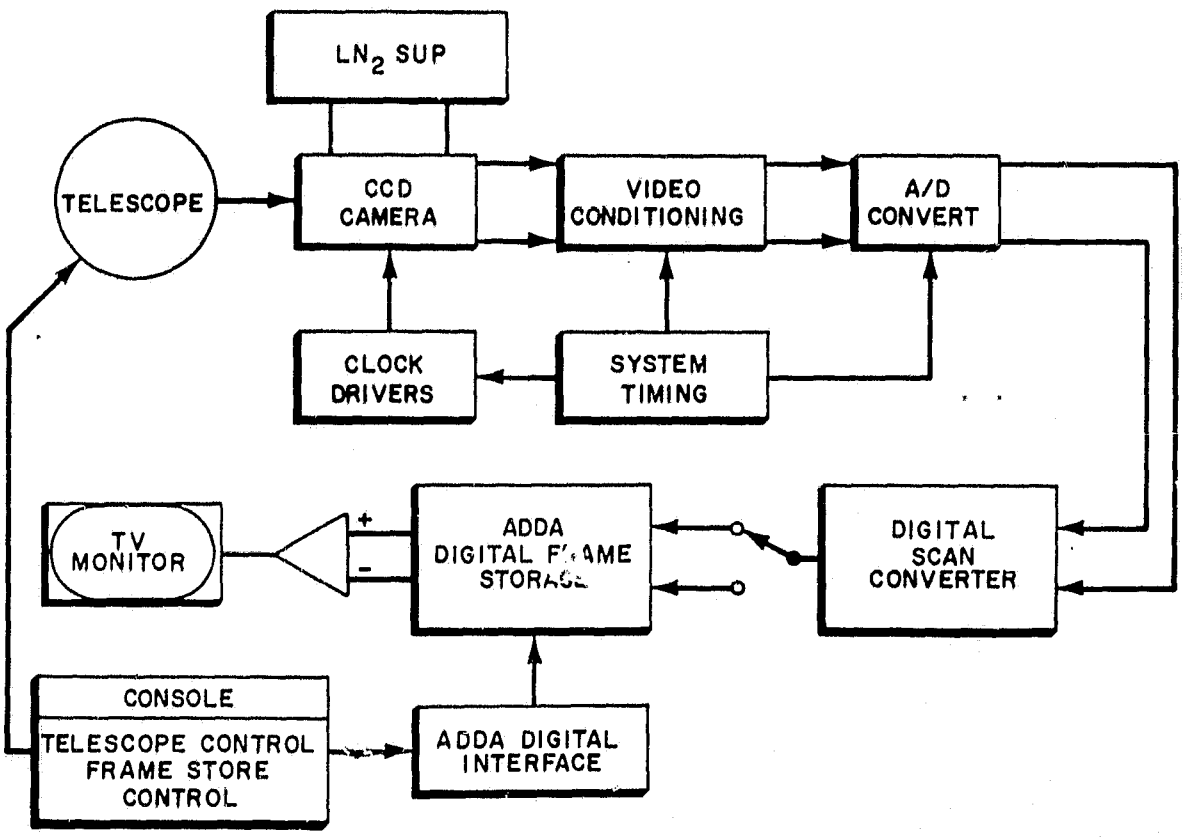

Figure 17. Two-element CCD camera system.

The limiting magnitude of V = $17^{m}.7$ is a function of the telescope, the CCD properties, and the integration time. With 2 CCD chips, instead of 6, these parameters would not change but the scan coverage rate would be reduced by a factor of 3. Moreover, we would not need additional video processing hardware as the current equipment would suffice. As can be seen from Table III this smaller scale design still represents a considerable improvement over current searches.

The principal piece of hardware that will be needed is a digital scan converter. This is necessary to adapt the CCD's 512 x 640 "slow scan" pixel format into a standard 480 x 640 television format at standard television frame rates. This, too, was necessary for the Air Force's use but would require modifications for the minor planet application. The final asteroid system is shown in Fig. 17.

To summarize, a V = $17^{m}.7$ (B = $18^{m}.5$), 200 square degree per hour camera system based on the RCA CCD chips was developed. It was maximized in commonality with the GEODSS retrofit camera to minimize its costs. It was expected to have had this system in operation at the ETS early in the fall of 1982. Unfortunately, CCD chip procurement lagged. We have been forced to switch to British General Electric chips and the delay caused us to miss the 1982-3 observing season. The new camera is operational now and appears to have almost the operating parameters originally predicted.

III. PLANNING AIDS

A. Old

The fundamental source of data on asteroid positions and orbital element sets is the Ephemerides of Minor Planets (EMP) published yearly by the Institute of Theoretical Astronomy at Leningrad. Until the 1980 edition the epoch of an individual orbital element set depended on the last time someone refined that orbit. Hence many element sets were quite old (1950s or 1960s with a fair number 10 - 20 years earlier). Therefore, without sophisticated numerical integration, these are useless for predicting positions. Also, as asteroids dim rapidly with increasing phase angle (about $0^m.03$/degree), observations are most frequent near opposition. Therefore the EMP includes geocentric ephemerides at 10^d intervals (for a time span of 70^d) centered on the instant of opposition for each asteroid undergoing opposition that year. These are in the form of 1950.0 right ascension (to $\pm\ 0^m.05$) and declination (to $\pm\ 0'.5$) at 0^h E.T. A simple computer program, which allows the user to specify the date of interest and the brightest asteroid of interest, was written to plan the observing. Since the ephemerides had to be put into machine readable form this aspect represented the huge bulk of work.

The output of the program, for all those asteroids undergoing opposition within 35^d of the requested date and sufficiently faint, is current epoch geocentric right ascension and declination, their rates, the position angle of the motion (to $\pm\ 5°$), the compass direction of the motion (e.g., NE or W), the last year seen, and the time to move 5" ($\pm\ 0^m.5$). This is given for both 0^h and 12^h E.T. of the requested date. The last quantity is indicative of the return time to the field (although the time to move 10" is probably better). The position and angular velocity were obtained by Lagrangian interpolation (3-point).

Starting with the 1980 volume of the EMP osculating orbital element sets for a modern date (currently 0^h E.T. December 27, 1980) are provided for each numbered minor planet. These can be used within a year or two of epoch to provide $\pm$ 5' pointing - the accuracy of the 10 day ephemerides. We already have this information in machine readable form and when coupled with the daily ephemeris of the Sun (already at the ETS) we can now treat pointing for asteroids in the same fashion as we do for artificial satellites. Once we've found a minor planet we obtain its position using standard ETS procedures. These are then reduced and published in the Minor Planet Circulars.

B. New

With the advent of regular asteroid observing at the ETS it became clear that an on-line planning aid for routine observations and an identification aid for both routine observing and minor planet searches were necessary. The planning aid (whose acronym became ASTPT from ASTeroid PoinTing) would be a non-real time program similar to the one used at the ETS for scheduling the observations of artificial satellites. The identification aid (ASTID) would be a program executed in real time. Since most asteroids are in essentially the same orbit (i.e., circular, in the plane of the ecliptic, 2.7 A.U. from the Sun) the identification space should be as large as possible. Hence provision to use position, angular velocity, apparent magnitude, color index, and lightcurve period would be advisable. Again there is a similar real time program at the ETS for artificial satellites.

The difficulty is the large size of the asteroid file - the current one contains $\sim$ 2900 entries and is rapidly growing. The current ETS (essentially high altitude) artificial satellite file has 502 entries. Moreover, execution

of the ETS correlation software frequently requires 20-25 seconds. Clearly something better in concept was needed and it was developed.

As noted above, since the return time increases as we progress into a 49 box scan, we routinely discover main-belt asteroids. Such objects are either catalogued, not catalogued but known, or unknown. The software described in Taff 1980 was taken and coupled to our on-line plotting facilities to serve both as a catalogued/not-catalogued discriminator and as a search secretary. The first thing done at the start of each night is to plot all of the tracks of every catalogued asteroid in the vicinity of our search region. Figure 18 shows an example of this. This overlay can be used as follows: on another sheet we plot the same part of the celestial sphere and block out the areas searched (e.g., the boxes of Fig. 19). Each MULSSC point (see § IV. B) is then plotted too (the dots in the boxes in Fig. 19) with a precision of 1'. Overlaying the other sheet provides an immediate identification for catalogued objects. Connecting several nights' worth of data yields the type of summary shown in Fig. 20. Catalogued objects are not followed after their identification. Non-catalogued objects are tracked for the duration of the search. Recently this software has been moved to our graphics display monitor for instantaneous updating during the course of the searches. R. C. Ramsey has been responsible for all of our real time aids.

C. Optimal Searches

There are three obvious places to search for Earth-crossing asteroids; (1) in the ecliptic, (2) at the equilateral Earth-Sun Lagrangian points, and (3) around opposition. One thinks of the ecliptic first because that is the orbital plane of the main-belt asteroids (mean inclination = 7°.9). This would

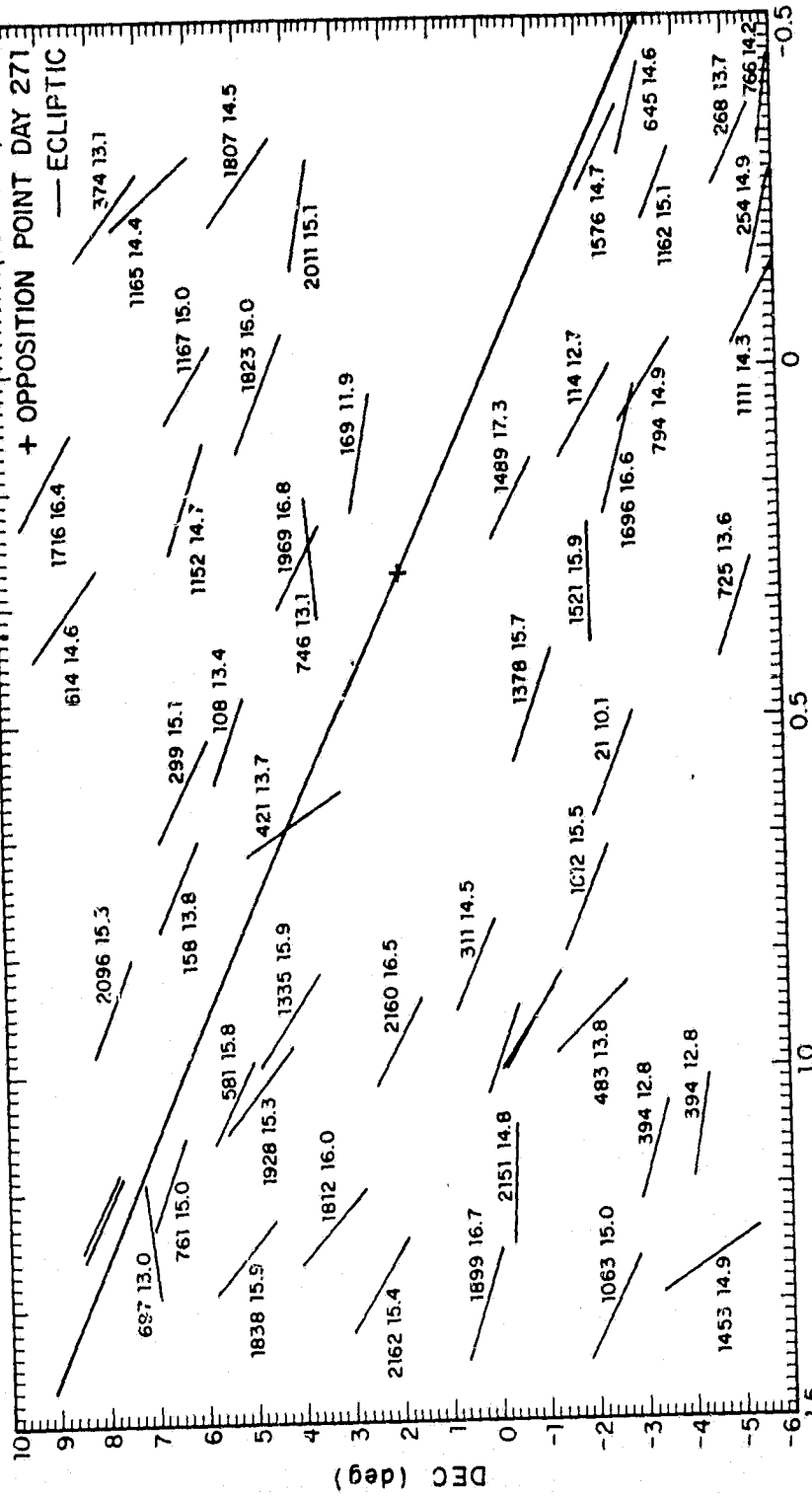

Figure 18. Predicted tracks of catalogued minor planets for the September, 1981 new moon.

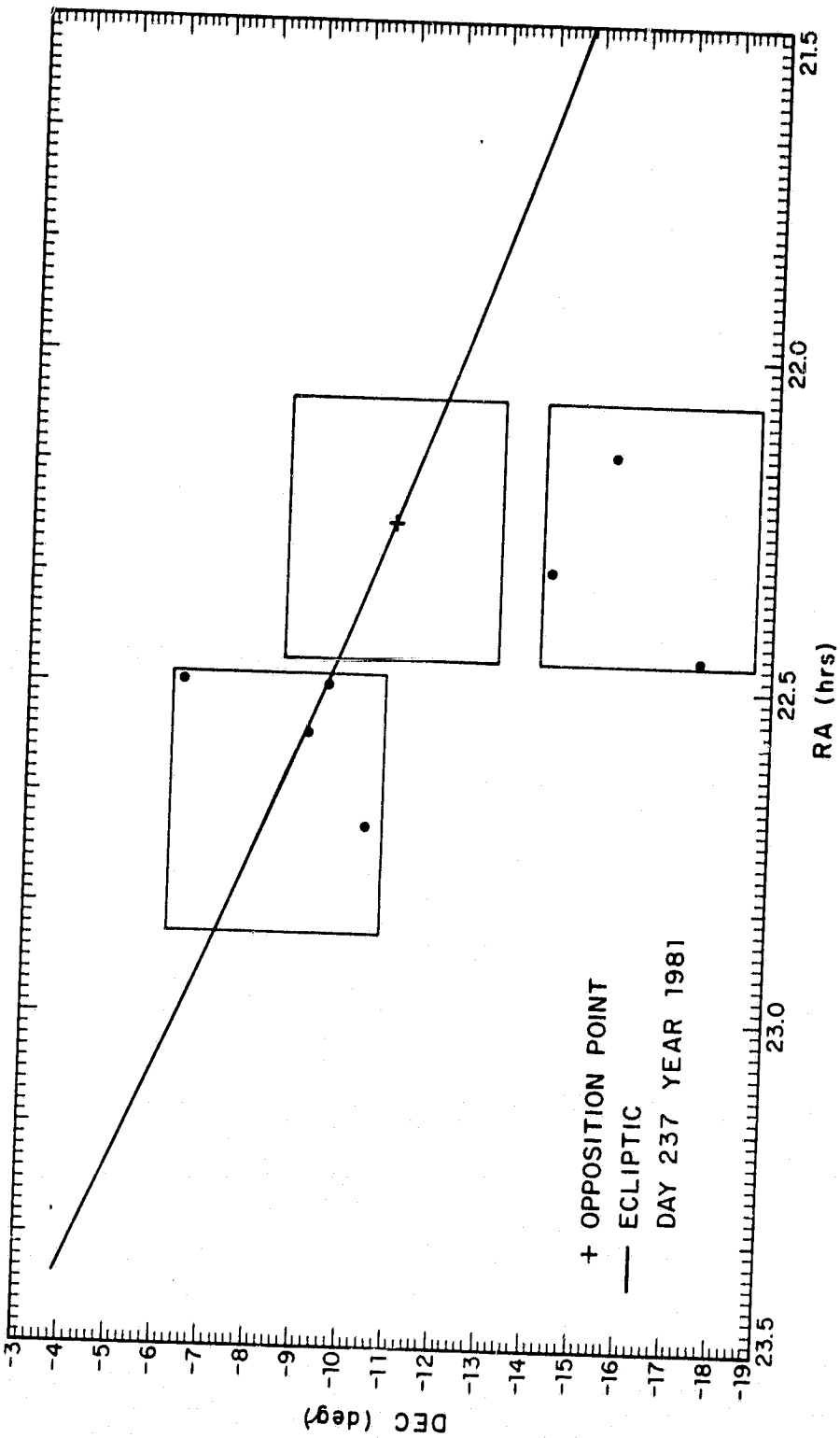

Figure 19. Areas searches (boxes) and data acquired (dots) on August 25, 1981.

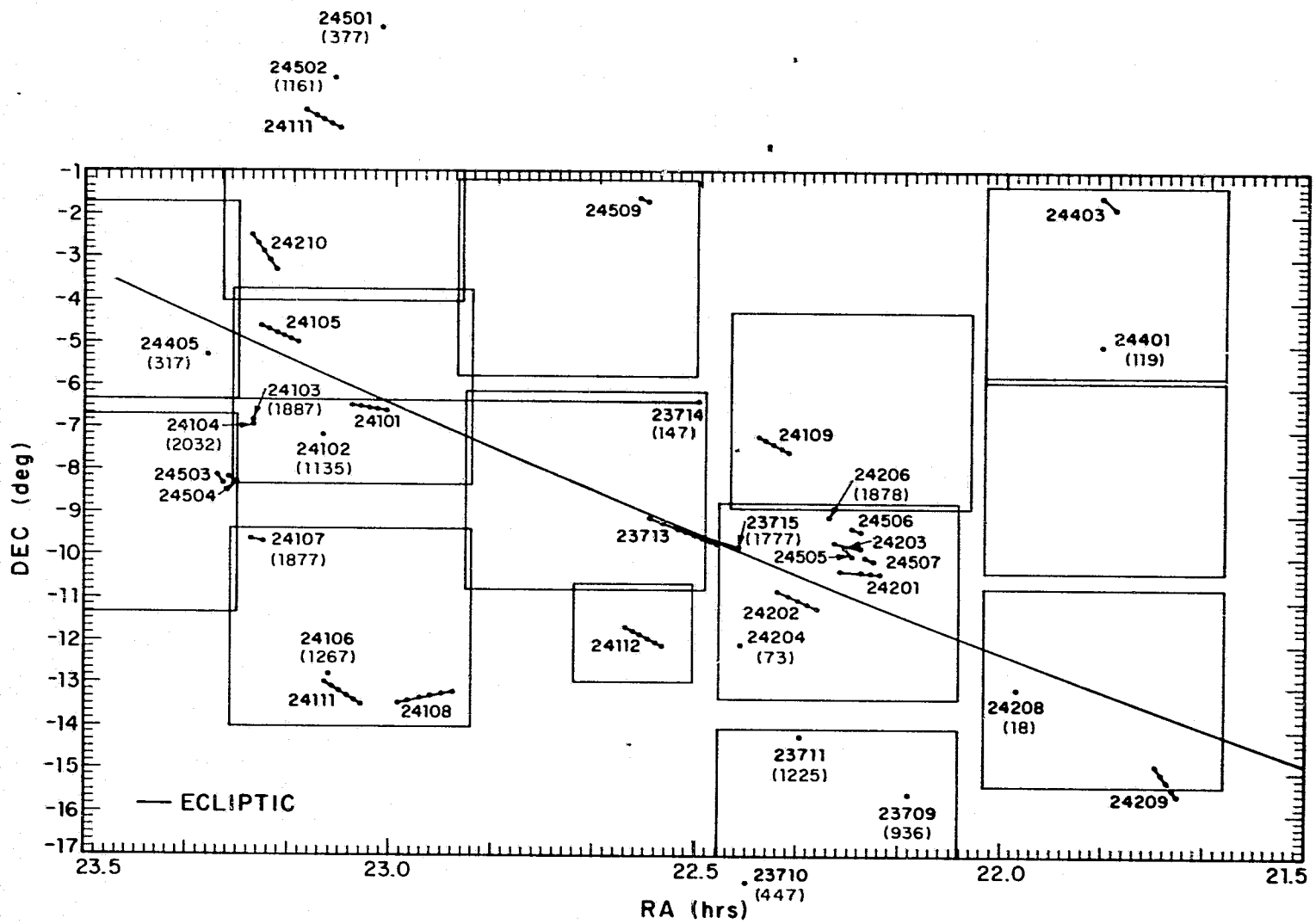

ORIGINAL PAGE IS
OF POOR QUALITY

Figure 20. Summary of all areas searches and data acquired for the August, 1981 new moon search.

mimic a near-stationary artificial satellite search. One eliminates the ecliptic because the known Earth-approaching asteroids have high inclinations (mean $\simeq 20°$) and parallax effects render an along the ecliptic search pointless.

The Lagrangian points come to mind next because there are asteroids at both of the equilateral Jupiter-Sun Lagrangian points (generically called Trojans). However the corresponding places for the Earth have already been searched with negative results. Thus there is opposition.

Opposition is that place on the sky directly opposite the Sun as seen from the (center of the) Earth. Hence, just as for the Moon, minor planets are their brightest when there. The linear part of the typical asteroidal phase function in magnitudes is $0^{m}.023$/deg so one need only go $\sim 22°$ from opposition before losing a half of a magnitude. Hence, at our most rapid search rate, we could cover half of this region in a night [$\pi(21°.7)^2/90$ sq. deg./hr = 16]. Since opposition moves during the night a good search pattern would be a non-overlapping spiral scan. Such a scan has been programmed and is using incrementally to cover the sky.

More for artificial satellites than asteroids it is very expensive and inefficient to waste telescope time. This follows because the satellites move faster than do the minor planets. Hence, especially in the design of searches, the concept of optimality has been introduced. Optimal search theory is a fairly well developed branch of operations research. Our group, for artificial satellite work, has invested several man-years of effort in this field lately and our asteroid searches have benefited. Most importantly we know and understand on a rigorous mathematical basis optimal asteroid

searches. We know how to execute them and why, we know what the payoff will be, etc. They turn out to be small ($\lesssim$ 10%) for the Earth-approaching asteroid search but the important point is our unique cognizance of the problem. See Taff 1983b.

IV. ASTROMETRY SOFTWARE AND ORBIT DETERMINATION

Until recently there were three different modes of acquiring accurate data at the ETS. Their acronyms are PLC, SSCSAO, and SSCFK4. The latter is no longer supported and there's now an amalgam of PLC and SCCSAO known as MULSSC. MULSSC has become the preferred mode of data acquisition on both artificial satellites and asteroids at the ETS.

A. PLC, SSCSAO, and SSCFK4

SSCSAO is a Single Star Calibration procedure utilizing the Smithsonian Astrophysical Observatory Star Catalog as the source of reference. The closest star to the program object in the SAOC is observed immediately after the program object. The telescopic position of the program object is then differentially corrected. SSCFK4 is identical in concept to SSCSAO but the source of reference stars was the much more limited FK4 and its supplement, the FK3SUP. SSCFK4 was always an analysis tool and is no longer supported.

PLC was designed to be a Precision Local Calibration procedure, modeled after the classical procedures of photographic astrometry. Its performance was unexpectedly poor. This failure has never been satisfactorily explained (unexpectedly poor means a total positional error >2-3"). Before the inadequacy of PLC for minor planet work was known a PLC point was the standard astrometric procedure for an asteroid. When the failure of PLC became clear, the standard astrometric procedure for asteroids was changed to three successive SSCSAO points. The average of this triplet (a normal point) was then used as a single "observation".

Before describing the modification that led to MULSSC it might be useful to explain the mechanics of a PLC operation.

We determine the position of any celestial object by adapting the classical methods of photographic astrometry to real-time operations. When the program object (asteroid here) is brought to the fiducial mark the observer pushes a button. This causes the computer to store the current position and time, search the SAOC for 5 (preferably, the minimum is 4) stars in the immediate vicinity (preferably <0°.53, the maximum is 0°.75), and displays a map of the surrounding 1°.5 including the brighter NGC objects. This electronically generated finding chart allows the observer to correctly orient himself. After all of this is done the computer directs the telescope, one at a time, to the reference stars. The operator completes the placement of the star on the fiducial mark and again pushes a button signifying the successful completion of the task. The software checks his judgment, stores the current position, and moves to the next star. Upon completion of this sequence, which requires 1-2 minutes, the linear "plate model" is constructed using the telescopic positions of the reference stars and their computed topocentric positions. One of the observed stars does not contribute to the model but is used instead to evaluate the systematic errors. Finally, the program object's position is deduced, stored, and printed. Experiments indicate that the overall precision is 4-5". This, in turn, is directly due to the digitized (≈6".5) control of the telescope that the operator has. Should an insufficient number of reference stars be in the area of the minor planet, this procedure is inhibited and a single star can be used to differentially deduce a less precise position for the asteroid (e.g., SSCSAO). Rapid repetitions of SSCSAO can be used to reduce the random errors.

After the switch in astrometric observing procedure (from PLC to the 3-SSCSAO sequence) the quality of our data improved rapidly. However, in a few (≤5%) cases, although our internal variance about the mean was small, our external systematic error would be large and variable. There are two simple causes for this in the 3-SSCSAO procedure that we can't discern at the telescope. One is an incorrect value for the reference star's position in the SAOC. As SSCSAO is a differential technique, such a systematic error will be propogated directly into the minor planet's position. The other is an incorrect star identification, replicated three times. Hence, to alleviate both of these problems MULSSC was created.

B. MULSSC

The reason one needs a new calibration routine for the asteroids is that SSCSAO always takes the closest star to the program object's position and over the execution time of SSCSAO (20-30 seconds), a minor planet doesn't move (0".62 in 30 seconds for an asteroid moving twice as fast as a typical main belt asteroid). Therefore in the 3-SSCSAO sequence the same star will be automatically chosen for each repetition. MULSSC uses the front end of PLC (which used 4-5 different stars for its reduction) to perform the asteroid-star sequence three times, but on three different stars. Thus, all the advantages of the SSCSAO triplet are preserved and the aforementioned potential sources of systematic errors eliminated. MULSSC stands for MULtiple Single Star Calibration. Finally MULSSC will execute more rapidly than would 3-SSCSAO procedures because of the reduced overhead.

The switch from PLC to 3-SSCSAO points was made in May of 1981. MULSSC was designed in November of 1981 and was operational in December of 1981. MULSSC yields results accurate to 2".5.

Until December of 1981 all calibration procedures updated the mean position of a reference star to its topocentric place and used that in modeling the telescope (for were the telescope a perfect optical instrument and all the mean to topocentric reductions perfectly performed then the computed topocentric place would be identical to the observed place). Starting with January 1, 1982 all procedures will skip the intermediate mean to topocentric then back to mean computations. This change is invisible to the observer.

C. Initial Orbit Determination

Our mode of observing, and especially astrometric data acquisition, is unprecedented in astronomy. We can acquire truly independent positional measurements on an asteroid as soon as it moves far enough that different reference stars are used (say 0.25). Moreover since the rate is unaffected by the actual time necessary to perform the observations, data rich initial orbit determination methods are feasible. When coupled with the fact that Gauss did not solve the angles-only initial orbit determination problem, much theoretical and numerical work was necessary. Once again, since all of these comments refer equally well to artificial satellites, planetary science has been forwarded at no expense. I shall not dwell on the details here, see Taff and Hall 1977, 1980 and Taff 1983a.

V. IMPROVEMENTS-THEORETICAL

In the latter half of 1981 the Space Surveillance Group of Lincoln Laboratory conducted an Earth-approaching asteroid search study. About two man years of effort were devoted to this project. Since we encompassed the existing artificial satellite search and observation expertise, we assumed that we could successfully tackle the asteroid problem too. In a nutshell the final conclusion was that no significant improvement could be made over the searches already being conducted or planned for the ETS. The design parameters are listed below that define significant. It includes increases in both scan coverage rate (by a factor of 2-3) and limiting magnitude (by a factor of 2-3 too). The essential difficulties are due to stars just below your limiting magnitude (whatever it is) and misregistration problems from the subsequent passes of the telescope. Neither one of these difficulties can be overcome without giving up scan coverage rate or sensitivity. We do feel however that one or the other can be sacrificed for an automated system.

A. Introduction

Studies were conducted in the Space Surveillance Group to pursue the design, construction, and operation of an asteroid search system based on technologies developed for potential improvements in the performance of the GEODSS space surveillance system. The overall objectives for the design include improved performance in limiting magnitude and search rate compared to all existing and planned asteroid search programs using relatively advanced sensor and detection processor technologies and the existing telescope and computer facilities at the ETS. First we provide a summary description of the preliminary baseline design of the asteroid search system, an initial

analysis of predicted performance, and a summary of design and implementation uncertainties that were subsequently being evaluated.

The asteroid search task of interest deals with the discovery of minor planets as faint as V = $17^m.8$ (B = $18^m.5$) having Earth-approaching orbits. These non-mainbelt asteroids have relatively fast geocentric angular motion (1 to 10 arc sec per minute) compared to main-belt asteroids which permit angular speed filter elimination of detections of main-belt asteroids. The Earth-approaching asteroids have orbits as viewed from Earth that require a full celestial sphere search coverage rather than limited searches. Other system performance goals include:

- Scan coverage rate $\geq$ 250 sq. deg. per hour
- Probability of detection $\geq$ 0.9 at full sensitivity and $20^m.5$/arc sec^2 sky background
- Automatic detection false alarm rate $\leq$ 5 per night.

The semi-automatic searches should run about 6 to 7 hours per night, seven to ten consecutive nights per month, with an anticipated discovery rate of about one object per week.

B. First Design

The design of the asteroid search sensor includes the facilities of the ETS except for the existing EBSICON cameras. It is assumed that one of the 31" telescopes with associated mount and dome system would be used along with the two MODCOMP-IV computers, one for telescope control and the other for real-time data recording and detection processing. A low-light-level CCD camera would be designed for the sensor. It will provide the required sensitivity, scan coverage rate, and image registration stability.

The CCD imager developed in the Microelectronics Group of Lincoln Laboratory for the GEODSS program is the basis for the camera design along with fiber optic tapered bundle (FOTB) elements. These permit the assembly of a mosaic of several CCD imaging chips on the focal plane with optimum pixel size. The high performance CCD chips are presently available for the asteroid sensor development.

Low-light-level CCD cameras can be operated in two modes; stare mode as in the case of a TV camera and image-motion-compensation (IMC) mode also referred to as time-delay-integration (TDI) mode. In the IMC mode the telescope scans the sky at a constant rate and the charge transfer mechanism in the CCD is clocked to be in synchronization with this rate. Integration of the image occurs on the CCD chips while the image scans across the CCD chip. In the stare mode the telescope searches or scans in a step-stare-step fashion requiring step and settle time. For a stare mode focal plane design the entire focal plane area is covered with a two dimensional array of CCD imagers (for maximum field coverage). Several frames of the field are clocked out for detection processing (requiring a shutter for the CCD's during readout). A loss of coverage rate due to readout time is therefore experienced. In the IMC mode only one row of CCD chips orthogonal to the scan direction is required for full coverage but additional rows of CCD chips are required in the scan direction for additional imaging of the field of view for multi-frame detection processing.

After all of these factors are taken into account, net scan coverage rate is about the same for both modes of camera operation. However, the IMC mode is preferred for the present design because few CCD chips will be required, therefore fewer parallel video and detection processing paths will be required,

less mechanical strain is experienced by the telescope and mount compared to the step-settle scan, and much less CCD responsivity normalization capability is required for IMC mode (per column of pixels) compared to stare mode (per every pixel). The IMC mode does require very stable telescope scans and very low focal plane distortion.

C. Sensor Concept

Within the guidelines discussed above, a preliminary sensor concept has been developed which should successfully achieve the asteroid search goals under specific conditions. In the design the CCD camera is operated in the IMC mode. This camera is located at the Cassegrain position on the ETS 31" telescope. The continuous scans would be in declination only from +30° altitude to near zenith with the telescope in sidereal drive. The resultant scan rate is such that all scans would occur essentially on the celestial meridian. As many as four IMC scans would be required for the same sky sector, each scan separated by about 15 minutes, to provide the time separated data for moving target indicator processing and the detection of the asteroids with respect to the star background.

Detailed descriptions of the CCD chips, CCD focal plane design, and detection processing functions are presented below. In addition to the present design two other configurations were considered. An asteroid search sensor design using an existing Lincoln Laboratory 5-CCD chip focal plane was analyzed with calculated performance results indicating no improvements over the present asteroid search capability. A design has also been considered with no fiber optic tapered bundles used in the CCD camera and the camera located at the prime focus position. This approach showed acceptable performance

levels but is less desirable because of the requirement for a larger number of CCD chips and associated processors versus the stare mode of operation.

D. CCD Chips

The CCD imaging device was developed in the Microelectronics Group of Lincoln Laboratory for the GEODSS program. The objectives were beyond the state-of-the-art low-light-level performance for a realistic IMC mode array geometry using proven silicon MOS device fabrication technology. The geometry of the 100 x 400 pixel large array device is illustrated in Fig. 21. For operation as an imager only, the active array, output register, and output on-package circuits are used.

The CCD imagers are fabricated using an n-channel process with two levels of polysilicon. An ion-implanted buried channel is used for high transfer efficiency and low noise, and an additional implant is used to provide a threshold voltage offset for two-phase operation. The device is front illuminated through the polysilicon gates. Figure 21 shows an output register to transport the charge to a conventional floating diffusion output circuit which provides charge-to-voltage conversion. This on-chip circuit is the source of electronic noise in the CCD. An emitter follower output circuit is included in the CCD package as a video buffer and line driver.

The pixel size is 30 x 30 μm, of which 84% is active channel and the remainder is channel stop. The chip area is 48 mm^2. Important aids in the evaluation of the device are two electrical inputs. An input register enables the device to be used in the serial-parallel-serial mode, and an input to the output register is also available. These features provide a

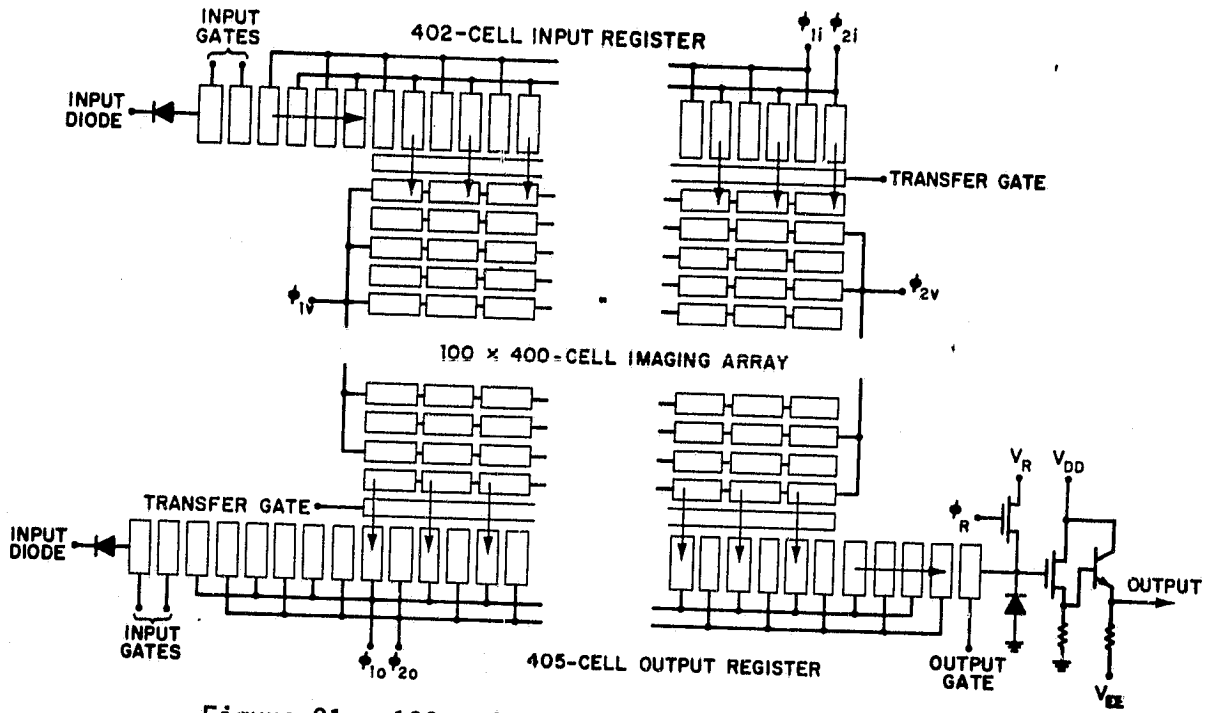

Figure 21. 100 x 400 element CCD array for GEODSS.

means of evaluating the charge transfer efficiency of the imaging and output registers.

For this application special attention must be paid to achieving high sensitivity down to very low signal levels. The principal factors affecting sensitivity are the optical responsivity, the charge transfer efficiency, and the device noise. Table IV is a summary of the present status of the CCD characteristics which have been demonstrated with a representative number of devices.

E. CCD Focal Plane Mosaic

The existing EBSICON camera faceplate (at the ETS) provides focal plane coverage over a 3.15 inch diameter circular area. Photographic plates indicate that the 31 inch telescope, Cassegrain focal position may have a useful focal plane greater than a 5 inch diameter circular area. In order to take full advantage of this telescope coverage capability, a mosaic focal plane of the CCD chips described above is required. Several rows orthogonal to the scan direction of staggered CCD chips across the width of the focal plane could be used. However, the telescope plate scale factor is such that pixel angular size would be very small ($\sim$1.6 arc sec) compared to nominal good "seeing" for point objects of about 2.8 arc sec. The straddle loss due to these small pixels would greatly reduce the electro-optical sensitivity. (The straddle losses were worked out by Don Batman.)

The use of fiber optic tapered bundles as optical reducers permits a selectable increase in pixel size at the focal plane as well as two dimensional abutting of active areas of the CCD with sufficient taper ratios, see Fig. 13. The effective increase in CCD active area also greatly reduces

TABLE IV

CCD REQUIREMENTS AND STATUS

	100 x 400 CCD Characteristics	
	Goal	Status
Dark Current (nA/cm^2)	5	<5
Transfer Efficiency	0.99992	0.99998
Noise (electrons)	20	12
Quantum Efficiency (percent)	40	35 to 40
Dynamic Range	10^4	$\simeq 2 \times 10^4$
Defective Columns (percent)	<5	$\simeq$ 1.8

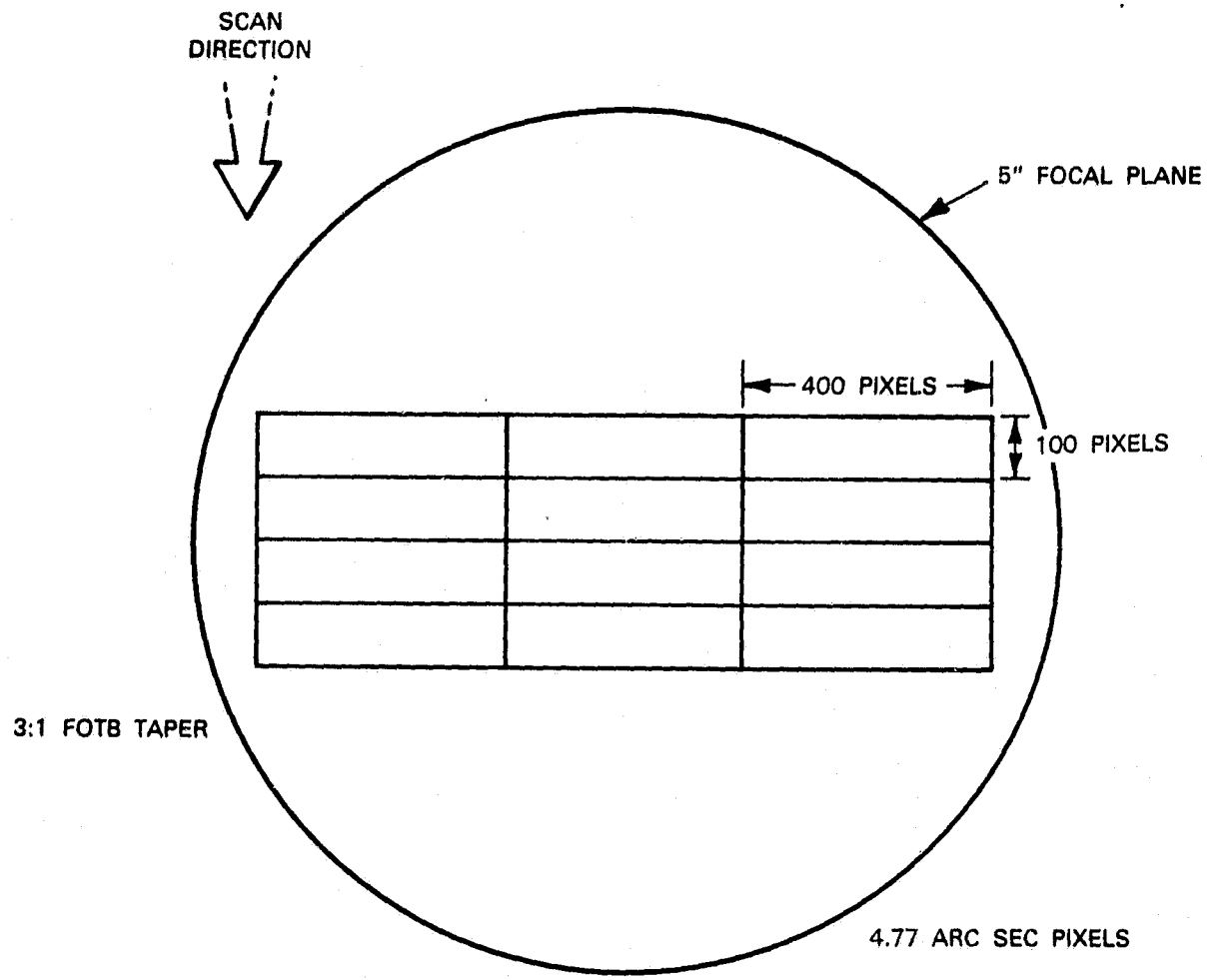

Figure 22. CCD-FOTB focal plane mosaic.

the number of CCD chips and parallel signal processing required for full focal plane coverage.

The designed CCD-FOTB focal plane mosaic geometry is shown in Fig. 22. The telescope plate scale factor of 0.75 mils/arc sec yields a CCD-FOTB pixel angular size of 4.77 arc sec if a 3:1 taper ratio is used for the FOTB's. For this pixel size and the 2.8 arc sec seeing, the pixel straddle loss is expected to be less than $0^{m}.25$ on the average. The 3:1 FOTB's also permit continuous coverage of the IMC scanned field with just three CCD's essentially covering the 5 inch telescope focal plane width. This results in a 1200 pixel wide scan.

In the scan direction four CCD-FOTB imagers are serially placed for each of the initial three parallel imagers to provide four separate, sequential measurements of the field-of-view for noise reduction as part of the asteroid detection process. The CCD-FOTB imagers are also abutted in the scan direction. (This is not necessary for the asteroid search but is desirable for possible use in detection of artificial satellites.)

The FOTB structure and interface to the CCD's result in a reduction in optical path transmission to about 58%. It is anticipated that thin optical fiber wafers would be used between the FOTB structures and the CCD imaging active front surfaces to permit the non destructive replacement of CCD's bonded to the FOTB's. The optical transmission for the wafers and interface is about 78%. These losses were modeled as a reduction in quantum efficiency of the CCD imagers.

For the IMC mode of operation the image of the celestial sphere must remain stable during the scan and synchronized within a pixel not only for

the portion of the scan in the 100 pixel column of the CCD but also within the correct pixel as a function of time for the total of 400 pixels resulting from the four CCD's in the scan direction. All forms of optical distortion associated with the telescope optics as well as the FOTB elements must be reduced below a specified minimum to support the rectilinear requirements for these IMC scans.

The present 100 x 400 pixel CCD imagers have been used in standard 24 pin device packages which are too large to permit abutting as called for in the FOTB focal plane structure. New alumina substrate packages would have to be fabricated for the existing CCD chips for this application.

F. Sensor Functional Description

The main sub-systems for the proposed asteroid search sensor are shown in the overview system block diagram in Fig. 23. The continuous (unframed) analog video stream from each of the twelve CCD-FOTB imagers would require some analog video conditioning at the 53 kHz pixel rate before analog to digital conversion. The asteroid detection processing functions can be separated into two categories: In-scan processing and Multi-scan processing. For the In-scan processing, several operations are applied to the digitized video, real-time: (1) CCD fixed pattern (or responsivity normalization) with pre-stored values for gain and DC bias per column per CCD chip is applied, (2) Single level adaptive threshold (e.g., constant false alarm rates) which may include the normalization function above are necessary, (3) All pixels with threshold exceedances are expanded to 2 x 2 pixel events to reduce sensitivity to pixel straddle and IMC scan instability, (4) Stored distortion field patterns are applied to correct chip-to-chip rectilinear pixel misalignment

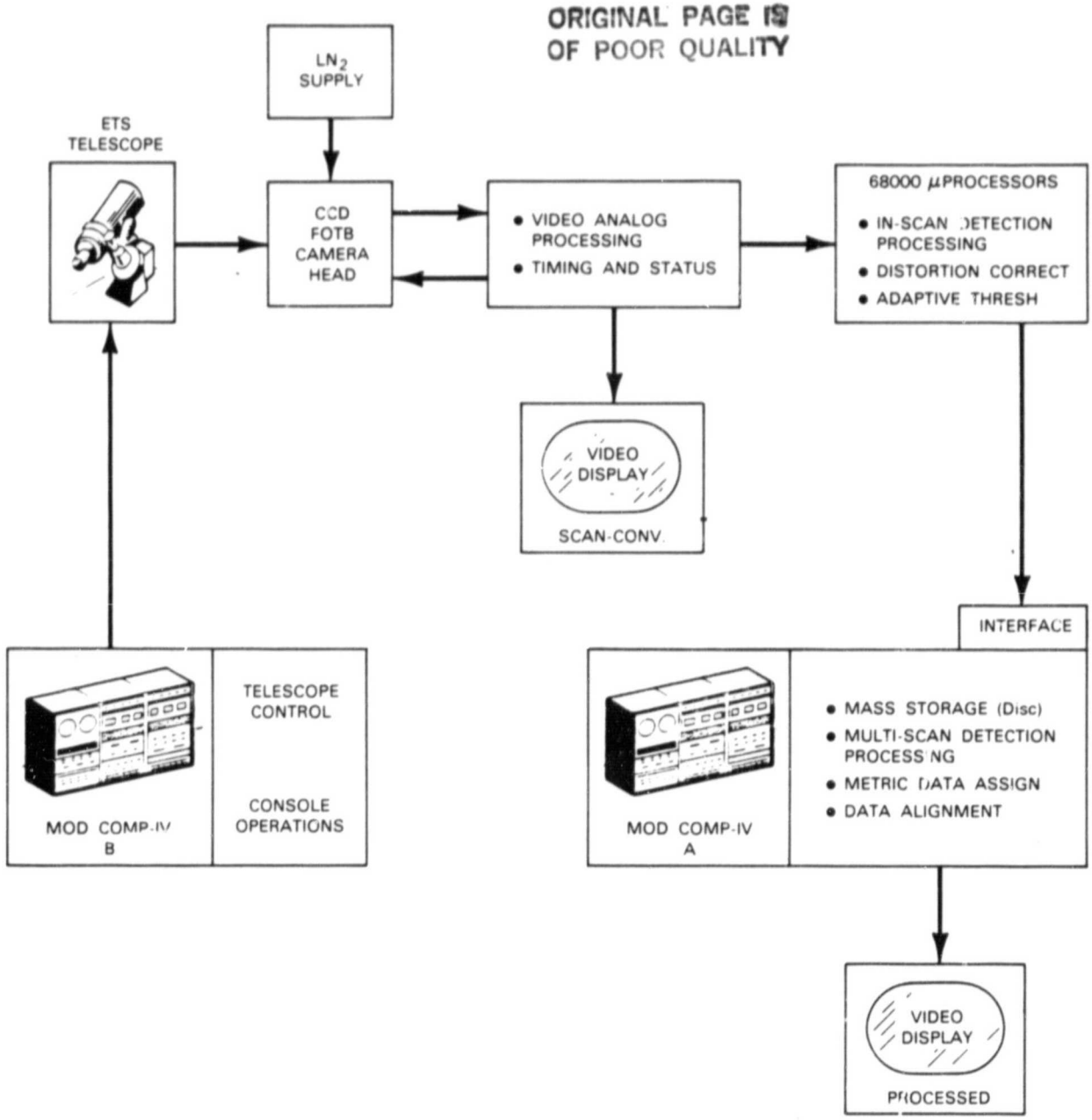

Figure 23. CCD-Asteroid search system block diagram.

due to optical distortion effects, and (5) Video from the four chips in the scan direction is differentially delayed and then compared for spatial correlation to reduce exceedances due to electronic noise and night-sky background. A three-out-of-four test algorithm would be applied at this step. Pixels with exceedances that have spatial correlation for at least three out of the four chips are considered either asteroids or stars, all others are considered noise events and are dropped.

The above operations occur for all of the video during a scan. The output one bit video represents detected asteroids, stars, and a small number of noise exceedances. This output for each scan for three columns of CCD chips of the sky sector along with object position information are stored in a digital mass storage system. Since the minimum rate for asteroids of interest is one arc sec per minute, and since a minimum of three pixel motion would be desirable between samples for moving target detection (each pixel is 4.77 arc secs), multi-scans of the same sky sector can be separated by as much as 14.3 minutes. This implies that the IMC scan can continue for about 14 minutes before stopping and returning to the scan start point for a rescan of the same sky sector.

It is desirable that four scans be sequentially made of the same sky sector for automated detection of the asteroids. Therefore complete coverage of the fully scanned sector would take about one hour. Upon completion of the four scans, the Multi-scan processing operations are performed on the stored data while scanning of the next sky sector continues. The Multi-scan processing includes: (1) Automatic alignment for spatial correlation of all four sky sector scans is performed on a continuous basis throughout the stored data review, (2) All exceedances from the first of four CCD-FOTB chips are

expanded a selectable number of pixels (in two dimensions) to provide an initial field map, (3) All objects occurring in the second pass which spatially fall within a region greater than three pixels but less than 30 pixels from objects in the first pass are considered potential asteroids, all other objects (stars) are dropped, and (4) The test above gives an indication of asteroid rate and direction. To scans three and four are applied tests using 3 x 3 pixel boxes spatially located based on these rate and directions results. The result of this four-out-of-four test greatly reduces false alarms due to stars and noise.

The detections resulting from the In-scan and Multi-scan processing described above must be evaluated for final asteroid verification, ideally with the same sensor system and with no interruption of the search scans. These functions are performed as follows. If an object is detected after the Multi-scan processing, the object is revisited for a one second integration period with the CCD camera in stare mode each time the telescope is returned to the new scan starting point. These (four) short verification stops will be occurring during the breaks in the scanning of the second new sky sector following the scan of the sky sector in which the object was originally observed. The four one second stare frames accumulated over a one hour period are then reviewed simultaneously on a monitor by a system operator for final asteroid detection verification.

This semi-automatic detection procedure interrupts the search process for only a minute or two per night and permits an automatic system false alarm rate of up to one detection per hour. Not allowing this forces the automated detection false alarm rate up. Correcting for this places the

entire search outside the interesting realms initially discussed or beyond present technology.

Implementation of the detection processing and data recording requirements will not be addressed here. It was thoroughly investigated by R. Martinson and A. Wardrop (of the Space Surveillance Group) and found to be feasible.

It can be anticipated that the asteroid search system operator(s) will provide four important functions: (1) Align and initialize each sky sector scan, (2) Assist in the alignment for spatial correlation of the Multi-scan detection processing operations, (3) Evaluate system detection for asteroid verification, and (4) Monitor functional system operation. Some of these tasks may be concurrent.

G. Electro-Optical Performance Estimate

For the most part the components and subsystems for the electro-optical portion of the system described above have been characterized in laboratory measurements and, in some cases, in field tests at the ETS. This experience makes possible the modeling and useful calculation of the potential electro-optical performance for this system design. Table V lists the important characteristics for a prediction of system sensitivity. For the required asteroid search scan coverage rate of 250 square degrees per hour, 40,000 CCD pixels per CCD chip, 3 CCD chips across scan, and four scans per sky sector, the effective integration time of the signal on a chip is 0.76 sec with a scan rate of 0.17 degrees per second.

The calculated sensitivity versus system electro-optical signal-to-noise ratio (SNR) is shown in Fig. 24. With sufficient detection processing to

Table V

Performance Characteristics

Pixel size at focal plane	α = 4.77 arc sec
Pixel straddle loss	g = 0.8
Telescope effective aperture	A_T = 0.23 m^2
Net CCD quantum efficiency	q = 0.17
System electronic noise	n_e = 25 electrons, rms

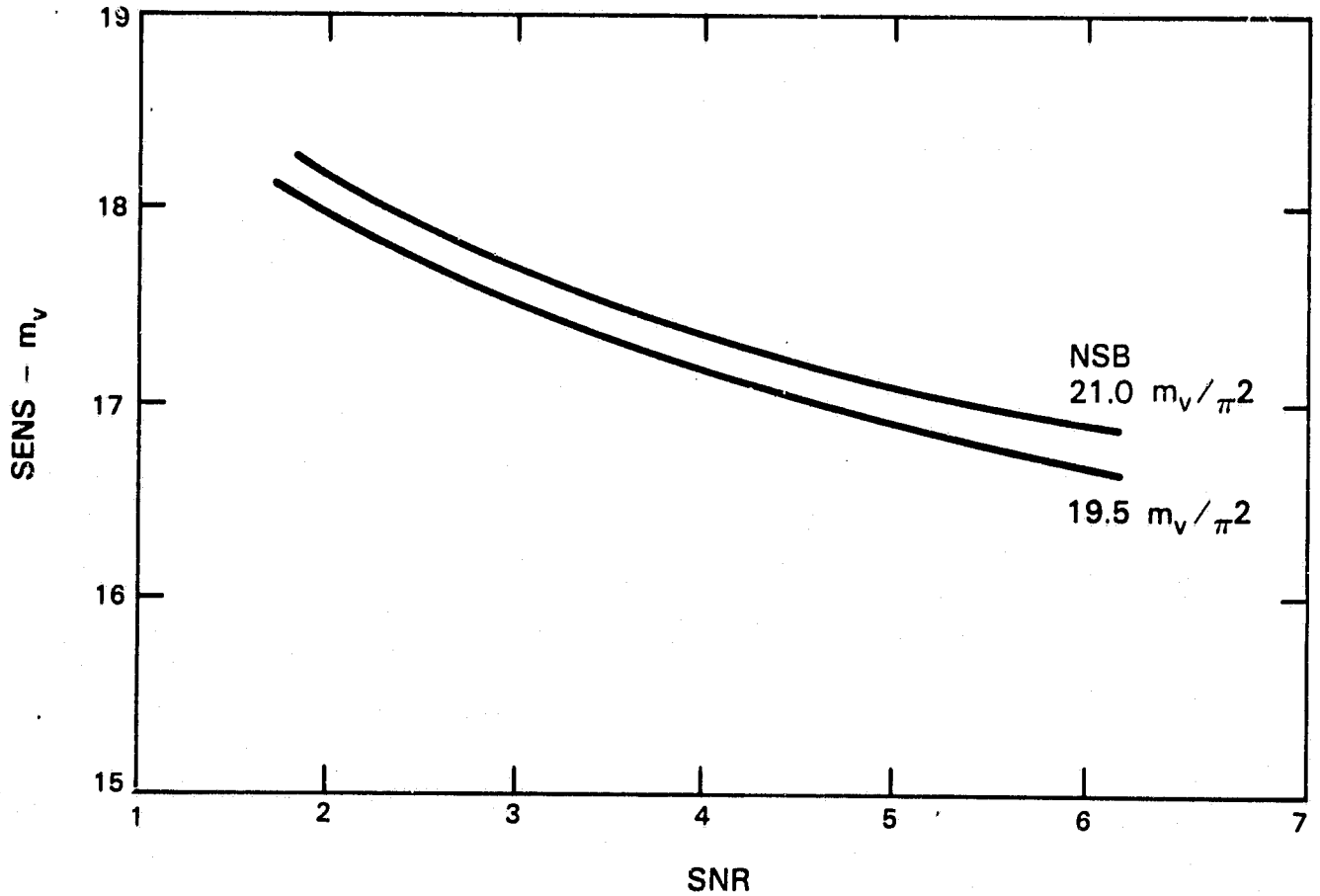

Figure 24. CCD asteroid search system electro-optical sensitivity.

permit system operation at SNR = 3 while simultaneously satisfying the probability of detection and false alarm rate goals, it is apparent from the calculations that the sensitivity goal of V = $17^{m}.8$ (B = $18^{m}.5$) should be achievable. An extensive evaluation of the detection sensitivity of the search system design is presented below.

H. Design Uncertainties

Several important design and implementation uncertainties exist at this time for the proposed asteroid search system. Some of these could be resolved following more detailed modeling and calculations, others may require more extensive investigation and measurements.

- For the IMC mode of search, the telescope scan must be very stable with very limited mechanical jitter or scan rate drift. The ETS telescopes are presently not stable to the degree required. Two possible solutions are: 1) to modify the telescope mechanical structures, or 2) develop an automatic pixel alignment function reacting real-time to scan instabilities during In-scan processing.
- Predictions of system performance changes as the search scans move through different density star backgrounds. Such complications would lead to a more realistic set of performance predictions.
- For these same reasons it would be desirable to calculate performance degradation versus actual seeing conditions anticipated at the ETS.

- Evaluation of distortion and other aberrations for the expanded 5 inch telescope focal plane would be desirable.
- The potential of fiber optic tapered bundles to provide sufficiently low distortion for the IMC mode needs to be determined.
- The total combined optical transmission loss for the complete FOTB-WAFER-CCD combination needs to be measured for the solar, two air mass spectrum and appropriate f/number system.

I. Performance Analysis

The physical instrument was described above. Based upon this a set of constitutive equations may be written. These equations relate sky-plane parameters, such as background brightness, to detection-plane parameters, such as mean signal level. They are:

$$\mu_0 = 10^{.4(15-m_0)} \Phi_{15} \alpha^2 \tau,$$

$$\mu_1 = \mu_0 + 10^{.4(15-m_1)} \Phi_{15} g\tau,$$

$$\Phi_{15} = A \int \theta F_{15} q \, d\lambda,$$

$$\sigma_0^2 = \mu_0 + n_e^2,$$

and

$$\sigma_1^2 = \mu_1 + n_e^2,$$

where

$\mu_{0,1}$ = mean (background, object) signal electrons,

$\sigma_{0,1}$ = standard deviation (noise) in (background, object) signal,

$m_{0,1}$ = (sky, object) brightness in magnitudes (per sq. arc sec),

A = telescope aperture,

θ = spectral throughput,

F_{15} = spectral flux from 15^m object,

q = spectral responsivity of detector,

τ = integration time,

n_e = equivalent r.m.s. noise electrons,

α = pixel size in arc sec,

g = loss due to finite pixel extent.

An additional parameter of interest is the scan coverage rate

$$SCR = \frac{WN\alpha^2}{P\ \tau}$$

where

N = number of pixels per chip,

W = number of chips across width of array,

P = number of passes required by system.

For the system described these become

$$\mu_0 = 10^{.4(15-m_0)} 4.99 \times 10^4 \tau,$$

$$\mu_1 = \mu_0 + 10^{.4(15-m_1)} 1.77 \times 10^3 \tau,$$

$$\sigma_{0,1}^2 = \mu_{0,1} + 625,$$

$$SCR = 188/\tau.$$

The operation of the system consists in eliminating the stellar background so this simple detection model will ignore stars. Complications due to imperfect star removal will be addressed later. An average background pixel contains a signal μ_0 with variance σ_0^2. A decision as to whether a pixel is occupied (ON) or empty (OFF) is made by setting a threshold T and reporting ON if the actual signal is at least T. Such a report is a false detection and occurs with a probability

$$f = \frac{1}{2} [1 - \text{erf } t_0]$$

$$t_0 = \frac{T - \mu_0}{\sqrt{2}\ \sigma_0}$$

An average occupied pixel contains a signal μ_1 with a variance of σ_1^2. Its state will be reported OFF if the actual signal is less than T. This error is a miss and occurs with probability

$$m = \frac{1}{2} [1 - \text{erf } t_1]$$

where

$$t_1 = \frac{\mu_1 - T}{\sqrt{2}\,\sigma_1}$$

It is frequently the case that $\sigma_0 \tilde{\sim} \sigma_1$. When this is so the detection statistics may be characterized by a signal-to-noise ratio

$$\frac{\mu_1 - \mu_0}{\sigma_0} \tilde{\sim} \sqrt{2}(t_0 + t_1)$$

Precise analysis, however, requires use of the distinct value of σ_1.

A reasonable set of design goals is 10^{-4} false detections per pixel and a 99% probability of detection. These goals lead to values of $t_0 = 2.63$ and $t_1 = 1.65$ or a signal-to-noise ratio of 6.1, just the sort of value usually associated with a (just) useful signal. The detection statistics can, of course, be improved by increasing the integration time. The concommitant loss in scan coverage rate, however, is not acceptable in the present application. An alternative is to form a column of n chips to obtain n sequential integrations of length τ. This procedure does not gain as much as increasing the integration to $n\tau$ because it adds in n readout noise contributions instead of just one. It does however realize much (in the present case $\sim$40%) of this gain and does not lower the scan coverage rate. The best treatment of, say, four samples is simply to add them pixel by pixel and then invoke the threshold. This, however, turns out to be difficult to implement at the appropriate rates. Almost as efficient and considerably easier to implement is immediate thresholding and then combination by three-out-of-four or four-out-of-four logic. Figure 25 shows

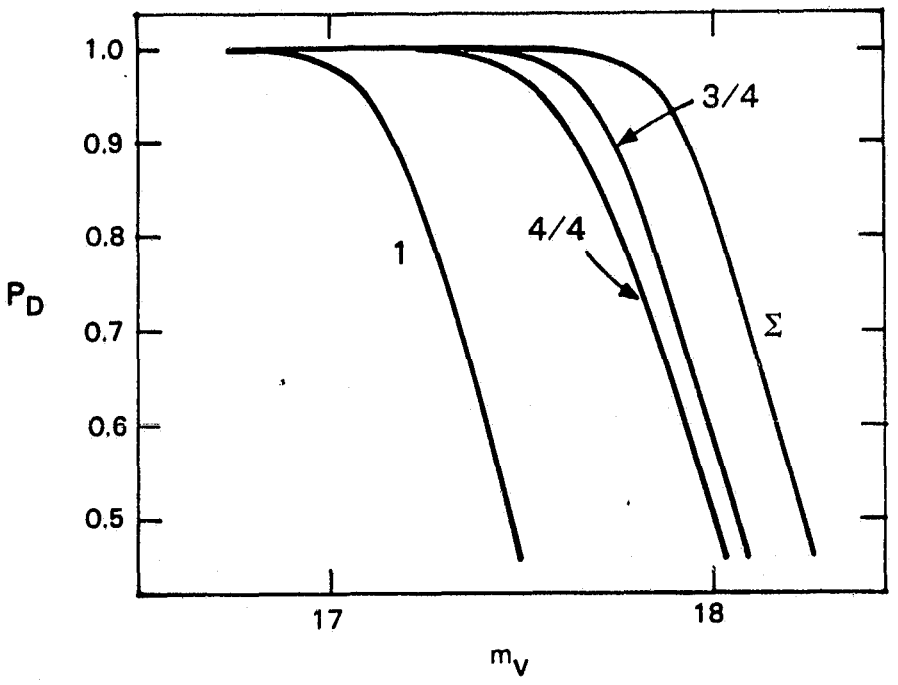

Figure 25. Probability of detection (P_D) as a function of apparent magnitude for several methods of data treatment.

probability of detection as a function of apparent magnitude for several data treatments; as indicated earlier the best treatment is direct summation followed by combination using three-out-of-four logic. The latter improvement in performance comes about because the requirements on the individual chip values for false detection f and miss m can be considerably relaxed while keeping the corresponding values for the entire column, F and M, at the specified values. For three-out-of-four logic the parameters are related by

$$F = f^4 + 4f^3(1-f)$$

and

$$M = m^4 + 4m^3(1-m) + 6m^2(1-m)^2$$

Hence for $F = 10^{-4}$ and $M = .01$ the corresponding single chip value $f = .0295$ and $m = .0420$ may be used. This leads to values of $t_0 = 1.33$ and $t_1 = 1.22$, or a signal-to-noise ratio of 3.6 for the data on a single chip. Note that this is somewhat higher than would have been needed if the full $\sqrt{4}$ gain of direct summation had been realized.

Those false detections present after the three-out-of-four logic may eventually give rise to system false alarms. This will happen when a set of false detections are arrayed in a series of passes in the same way a moving asteroid would be. Naturally, it is important to keep the rate of occurrence of these false alarms low. This rate may be approximated as follows: (1) First Pass: Probability of false detection in a given pixel

$$P1 = F$$

(2) Second Pass: Probability of false detection in a 31 pixel square region less a three pixel square region centered on first pass detection

$$P2 \approx 951F$$

(3) Third and Subsequent Passes: Probability of a false detection in a three pixel square region projected from first and second detection

$$P3 \approx 9F$$

The product of these probabilities is the range of false alarms per pass per one pixel so that the overall occurrence is obtained by multiplying by the ratio of the coverage to the pixel area. An appropriate value for this ratio is 10^9 for a single night's observing. For $F = 10^{-4}$ and two passes the number of false alarms is $10^9 \times 952 \times 10^{-8} \sim 9500$ which is obviously much too high. A third pass adds a factor 9×10^{-4} reducing the number of false alarms to ~ 8.6 which is still somewhat high, and a fourth pass reduces the number to about .0077, a satisfactory value. For $F = 10^{-5}$ the number of false alarms after three passes is about .0086.

Characteristics were calculated for a nominal system defined as follows: (1) Focal plane consists of three columns of four chips, (2) Single pass detection via three out of four logic, (3) Asteroid detection on four successive passes, and (4) $F = 10^{-4}$ and $P_D = 99\%$. Maximum was calculated as a function of scan coverage rate for sky brightnesses of $19^m.5$, $20^m.5$, and $21^m.5$ per sq. arc sec. Characteristic curves are plotted in Fig. 26. The value chosen for g (0.8) is appropriate for typical seeing (2-2".5) at the ETS. It must be noted that this assumes no contribution from telescope vibration.

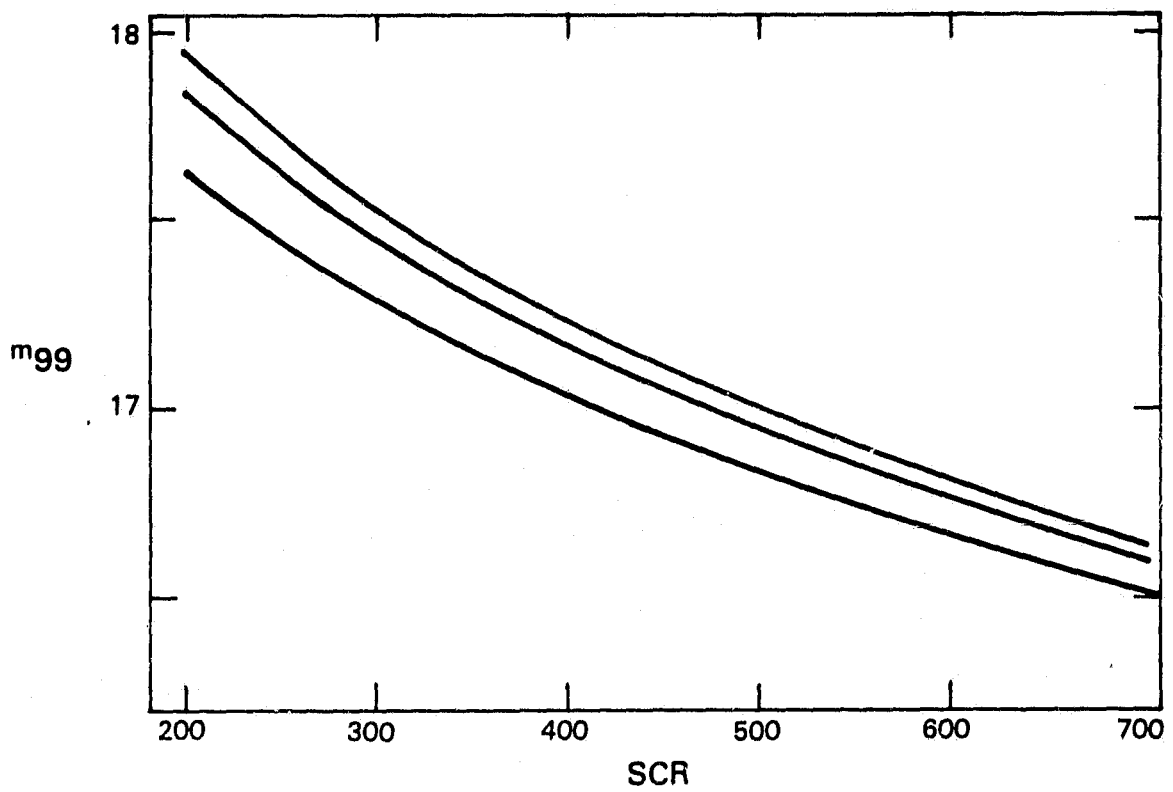

Figure 26. Apparent magnitude for a 99% probability of detection (m_{99}) vs. scan coverage rate (SCR), in sq.deg./hr. The three curves are for night sky background brightnesses of $21^m.5$ (top), $20^m.5$, and $19^m.5$ (bottom) per squared arc second.

The magnitudes at which P_D = 50% are about $0^m.4$ fainter than those given by the 99% curves.

When the real properties of the sky background are taken into consideration two complications arise. The two types of loss of performance are decreased probability of detection and excessive false alarms. The star background is removed not by arithmetic subtraction, but by logical negation. Thus if a pixel contains a star that pixel will not be available as a possible asteroid location and so a certain fraction of the focal plane will not be useful. In fact a star will remove not just one pixel from use, but an entire three square array. The fraction of 'occupied' pixels may be calculated as

$$n_0 = 9 \int_{-\infty}^{\infty} A(m)\, d(m)\, dm$$

where

$A(m)\, dm$ = number of stars per pixel within magnitude range dm about magnitude m

$d(m)$ = probability of detection on one pass at magnitude m

and will be a function of sensitivity as parameterized by, for example m_{99}. Figure 27 shows a plot of n_0 vs m_{99}. If asteroid detection requires separate detections on four passes, then the detection probability is not actually 99% in Fig. 27 but must be multiplied by $(1-n_0)^4$. This is about 0.73 for $m_{99} = 17^m.45$.

Stars, like false detections, can also give rise to false alarms. This is because there are many stars which are so faint that they are only occasionally detected. These occasional detections, just as false detections, can be so arrayed as to produce a false alarm. Stars appropriate for participation in this sort of false alarm are those which are detected on one pass and are not detected on the other three passes. The rate of occurrence of these occasional stars may be readily calculated:

$$O = \int_{-\infty}^{\infty} A(m)\, d(m)\, [1-d(m)]^3\, dm$$

Figure 28 shows a plot of O vs m_{99}. Somewhat surprisingly, perhaps, it is apparent that occasional stars rather than false detections are the dominant source of false alarms. The overall rate of occurrence of these false alarms may be calculated exactly as was done for false detections. The result is about 3.8 per night. This rate can be tolerated, but is clear that these false alarms are a primary stress on the system.

J. Conclusions/First Design

It appears that it might be possible to build an asteroid detecting system with quite satisfactory characteristics. These are: (1) Scan coverage rate $\geq$ 250 square degrees per hour. A soft maximum around 400 is set by data processing and storage limitations. A secondary deterrent to higher rates is the increasing importance of the constant readout noise as integration time decreases, (2) Characteristic limiting magnitude V $\sim 17^m.9$ ($B \simeq 18^m.6$). At this magnitude the probability of detection is about 50% rising for brighter objects

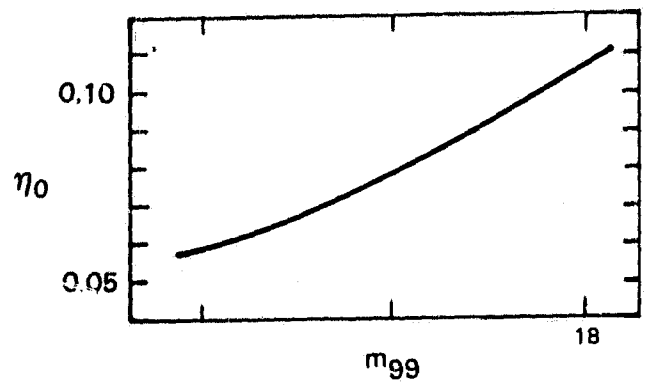

Figure 27. Star crowding as a function of limiting magnitude.

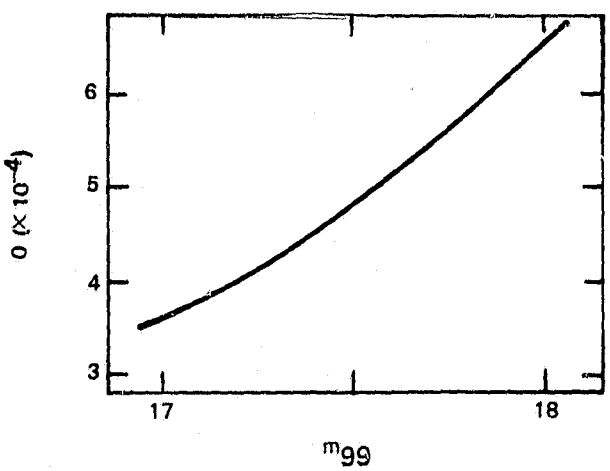

Figure 28. Occupation of pixels by stars vs. limiting magnitude giving rise to false alarms.

to about 73%, a value set by star crowding, and (3) Number of automatic system false alarms $\lesssim 4$ per night. These events are primarily due to the accidental linear arrangement of faint stars.

The candidate design for the asteroid detecting system is a reasonable tradeoff amongst sensitivity, false alarm rate, coverage, and complexity. At this point the performance is most strongly limited by the relatively small number of pixels. (Indeed a 1 inch square photographic plate exposed for a minute would reach fainter magnitudes and produce pixels more than three times as fast as this design would.) Major improvement thus awaits improvement in the telescope, CCD characteristics, and data handling capabilities.

K. Second Design

Immediately above a detection system based on the Lincoln Laboratory CCD used in the IMC mode was described. A set of system goals was postulated and the system was modified and adjusted to approach these goals. One of the disappointments in the evolution of the system design was the necessity of increasing the number of scans from two to three and then to four and possibly even five in order to deal with problems which came to light during the analysis. This not only severely reduces coverage but also introduces a new failure mode --parameter variation over the rather long duration of a detection. Clearly it is worthwhile to investigate the possibility of returning to a two scan detection scheme.

A key feature of the IMC system described above is thresholding very early in the data stream. This feature greatly eases the data handling load to the point where existing technology, largely off-the-shelf, is adequate.

The early thresholding, however, turns out to introduce a new set of problems, particularly in connection with the star background. An especially undesirable result is loss of detection probability even for bright objects.

The IMC mode of operation imposes some rather severe requirements on the system hardware. Unfortunately it is the nature of the system just described to fail catastrophically, either by going blind or becoming flooded with false alarms. Attempts to deal with sub-standard hardware in the processing stage tends to exacerbate other problems. In fact it is this interaction which has driven up the number of scan repetitions. Thus, there evolved some doubt that the processing hardware requirements could be met. Hence an alternate detection scheme conceived specifically to address the three problems mentioned above was developed. It is a step-stare system, so the IMC hardware problems are avoided. Where 'scan' appears in descriptions of the IMC system, 'exposure' will appear in this description. Thresholding is put off until the end, so the problems associated with early thresholding are avoided. This also allows noise problems to be handled simply by appropriate adjustment of the threshold so that detection can be performed with two exposures. A new problem introduced is a rather large data processing load. No attempt is made here to address the question of how to carry out the required processing (or even if it could be done).

L. Detection Characterization

This evaluation begins with a simple characterization of three candidate focal planes for a typical set of operational parameters. The three are the 800 by 800 device manufactured by Texas Instruments (TIS), the same device used with two by two on chip binning (TIB), and the 576 by 385 device

manufactured by British General Electric (GEC). (This is the CCD chip RCA's failure to delivery forced us to.) These are imagined to be mounted at the prime focus of the ETS 31 inch telescope. Operational characteristics are summarized in Table VI. Included are values of g, the loss due to finite pixel extent, for two representative values of the seeing measure. As above, the first approximation to characterization of the system will be to ignore problems due to stars. For the purpose of this characterization, search will be considered to consist of two exposures, of 7.5 seconds duration each, separated in time by several minutes. Detection is made by subtracting the two exposures and thresholding the difference. Three additional parameters are relevant: (1) Telescope step and settle time 2.5 seconds, (2) RMS noise electrons 25, and (3) Sky brightness $20^{m}.5$/sq. arc-sec.

The rather long exposure time was chosen in order to keep the detector duty cycle high. If this value is decreased much then the sensitivity falls off rapidly with only a modest gain in scan coverage rate. In the absence of a figure of merit, expressed as a function of limiting magnitude and scan coverage rate, no quantitative optimisation is possible. It does, however, seem plausible to expect any optimum point to lie in a region with a high duty cycle. In addition, data handling considerations are likely to speak against significantly shorter exposures. Characterization was carried out by choosing an acceptable false alarm rate, setting a threshold which achieves this rate, and calculating the magnitude equivalent of the threshold. This was done in exactly the same fashion as was described above. It should be noted that the standard deviation in the difference is $\sqrt{2}\,\sigma_0$. Detections occur when two threshold exceedances, one on each of the two exposures, have

TABLE VI

DETECTOR CHARACTERISTICS FOR STEP-STARE METHOD OF ASTEROID SEARCH

	TIS	TIB	GEC
α(arc-sec)	1.37	2.74	2.01
A(sq. deg.)	.093	.093	.069
$\overline{q.e.}$	.5	.5	.4
$\overline{g}$(s = 2 arc sec)	.47	.69	.55
(s = 3 arc sec)	.29	.57	.46
N(sq. deg)$^{-1}$($\times 10^6$)	6.9	1.7	3.2

a separation within a specified range. If the exceedances are merely statistical fluctuations in the background then the detection is a false alarm. The rate of occurrence of these is given by the expression

$$f^2NM$$

where

f = probability of a single pixel exceedance due to noise,

N = number of pixels per square degree,

M = number of pixels in the association range.

Using values of one false alarm per 500 sq. deg. and 1500 pixels in the association range, f may be calculated for each detector. This in turn leads to a value for the threshold and, finally, an equivalent magnitude. The calculations are summarized in Table VII. The best performance is obtained for the TIB case, but the differences are really rather small. An object at the threshold magnitude has, of course, a 50% probability of being detected on one exposure and thus a 25% probability of forming an associated pair. For each of the three detectors an object $0^m.3$ brighter produces a signal 2.0σ, above threshold and thus has a 95% probability of forming an associated pair.

M. Step-Stare System vs IMC System

It would be interesting to compare the performance of the TIB detector with the IMC System. For this purpose a system of three TIB's was assumed. This choice gives a focal plane with the same number of pixels as the IMC focal plane and is thus, in some manner of speaking, an equivalent system. In fact the prime focus position at the ETS might accommodate as

TABLE VII

CALCULATION OF THRESHOLD EQUIVALENT MAGNITUDE

FOR SPECIFIED FALSE ALARM RATE

	TIS	TIB	GEC
μ_o	445	1775	765
σ_o	32.7	49.5	37.5
$f(x10^{-7})$	4.4	8.8	6.4
t_o	3.48	3.38	3.42
$T - \mu_o$	228	331	255
m(s = 2 arc-sec)	19.7	19.7	19.5
(s = 3 arc-sec)	19.2	19.5	19.3
σ_1	36.0	52.3	40.6

many as six TIB's. Integration time was allowed to vary so that sensitivity could be plotted against coverage rate, and sensitivity was parameterized by the magnitude needed to give 99% probability of forming an associated pair. A calculation was carried out for the case of one false alarm per 500 dq. deg. and a seeing measure of 3 arc sec. A comparable calculation was carried out for the IMC system, adjusting the equations above to the appropriate false alarm rate and seeing measure. The results are plotted in Fig. 29.

Reference to Fig. 29 makes it clear that the strength of the step-stare system is in a deep, relatively slow search while the IMC mode is the system of choice for less faint but more rapid searches. The location of the cross-over point depends upon the step-settle time, thus decreasing this time is a very effective way of improving performance. The coverage can, of course, be much increased by placing more chips on the focal plane.

N. Problems Due to Stars

As in the case with the IMC mode of search, the performance of the step-stare search is degraded by the presence of stars. The effects are crowding (which decreases probability of detection) and increased noise amplitude (which increases the rate of false alarms). Because the present technique keeps the full amplitude information, these problems are a lot less severe than they were for the system described above with its early thresholding. In this section these two effects will be dealt with qualitatively. A partial quantitative analysis is described below.

The stars are part of the background and will be subtracted out owing to their lack of motion. The standard deviation of the signal will, however, be greater for pixels containing a star. These pixels will thus exceed the threshold more often and give rise to an unacceptably high false alarm rate.

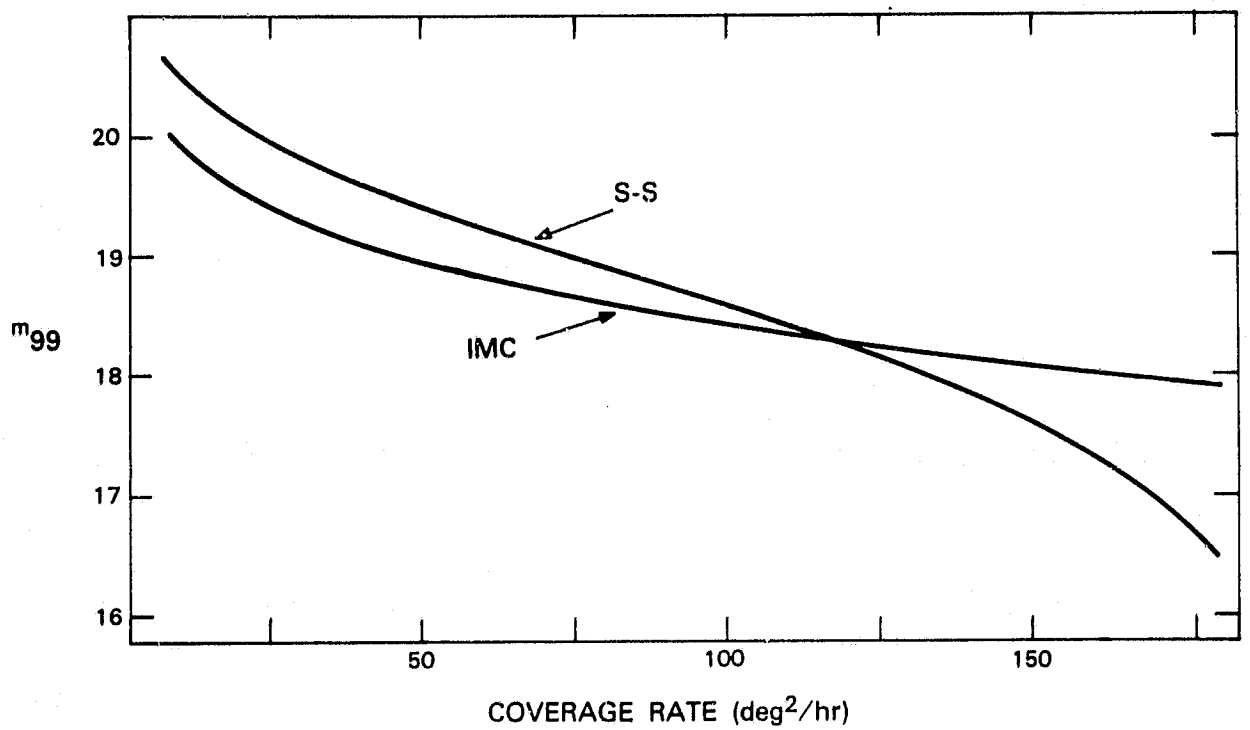

Figure 29. Comparison of 12 LL CCD chip IMC search and 3 TI CCD chip step-stare search.

In the IMC system this problem was dealt with (essentially) by ignoring all data for pixels occupied by stars. This was done concommitantly with the early thresholding and not for the purpose of reducing false alarms. In fact this technique led to high false alarm rates (due to marginally detectable stars). A second way of dealing with the increased standard deviation at star locations is to raise the threshold in response to the increased signal at these locations. In order to keep this technique from wiping out detections of fainter asteroids, the signal which drives up the threshold should be the lesser of the two exposures. Since the asteroids move, this signal will be just the sky background, leaving the background threshold in effect.

In the IMC system the excision of star locations combined with the four scan technique led to a rather large loss of detection probability for all asteroids. The present scheme improves on this both by being a two exposure system and by keeping the full amplitude information. After the stars are subtracted the only remaining evidence is the increased noise at the former location. Of course when the threshold is increased to cover the increased noise the probability of detection will decrease. This is certainly no surprise. Interference by a 15 magnitude star should decrease probability of detection for an 18 magnitude asteroid. But this is vastly superior to the IMC situation where an 18 magnitude star could mask the presence of a 15 magnitude asteroid.

A final problem is misregistration. This problem was not attacked for the IMC system; a likely 'solution' is growth of all detections (real and false) which worsens the false alarm rate and crowding problems. In the present case misregistration by a fraction of a pixel will lead to excessive

residues at star locations after subtraction. This sounds like a repeat of the noise problem and thus can be treated the same way. In this case, however, the threshold will need to be a stronger function of signal thus worsening the mild crowding problem. Clearly the 'right' thing to do is obtain correct registration. The difficulties associated with doing this must be traded off against the performance loss associated with raising the threshold.

O. Numerical Simulations

Characterization of detection performance makes use of strongly nonlinear functions. One result is that the mean value of a function generally differs from the function of the mean value. A simple example is the fact that the mean location of a star image is the center of a pixel while the mean integral of the intensity over the pixel is considerably less than the integral calculated for the centered position. This is the straddle loss. The use of mean values, such as g, in the calculations is thus suspect. It is straightforward to formulate the problem correctly but the integrals can not generally be evaluated analytically. The problem becomes particularly acute when effects due to stars are included.

There are two ways of dealing with this problem. First, and most straightforwardly, the appropriate integrals may be evaluated numerically. A second course of action is to devise a numerical simulation of the detection system and to compile statistics by performing experiments on the simulated system. This second course has the advantage of providing interesting and intuitively helpful intermediate results, and is the method chosen here. A set of programs has been written to simulate asteroid detection using a CCD detector. A full numerical investigation is beyond the scope of this report; a few applications of the simulation will be briefly described here.

The simulation program consists of four subsections. The first, MAPLET, produces a 100 by 100 pixel array with background and contribution from stars calculated for operator assignable pixel size and seeing. It assumes a normal intensity distribution for the seeing disk. Varying star densities can be assigned, and a full field offset may be added for investigating the effects of misregistration. The next two programs, ASTPUT and SUBMAP, can be used to produce a pair of small ten pixel by ten pixel arrays containing the same star background and an asteroid displaced by about three to four pixels. The SUBMAPs also contain appropriate statistical noise. A fourth program processes the two SUBMAPs to simulate the detection and false alarm reporting.

Two simulations of one hundred asteroid detections on the TIB detector were run. For the first the threshold was set so that the expected noise false alarm rate was extremely low. As described above the threshold was driven by the lesser of the two exposures so as to reduce star generated false detections while still maintaining a useful detection probability. For the second run the threshold was lowered so that some false detections might be encountered in the simulation. The results are summarized below:

		#1	#2
Asteroid Brightness		$19^m.0$	$19^m.5$
Probability of Detection		56%	57%
False	Expected	0	20
Detections	Found	0	21
False	Expected	0	1
Alarms	Found	0	0

The expected number of false detections is that calculated for noise with no contribution from stars. The agreement with the number found indicates that the thresholding technique will successfully deal with the stars. As an interesting sidelight it should be noted that an asteroid was inserted in every field of view, a rather unrealistic average. The study of star effects thus suffers from asteroid crowding!

A second application of the simulation package was used to look at the effect of misregistration. The two thresholds mentioned above were used again. No asteroids were included. The results are summarized below repeating the expected values from the previous table.

		#1		#2	
Misregistration		.2 Pixel		.3 Pixel	
Threshold		HI	LC	HI	LO
False	Expected	0	20	0	20
Detections	Found	20	59	35	89
False	Expected	0	1	0	1
Alarms	Found	2	16	8	35

The excess of found values over expected values represents the effect of misregistration. In this accounting a cluster of adjacent pixels over threshold, apparently due to one star, was counted as a single false detection. This is perhaps too optimistic; the total number of 'ON' pixels was about twice the number of false detections. The false alarms include several multiple false alarms. In practice new thresholding algorithms would be invoked to hold down false alarms at the cost of sensitivity. Apparently the effect of misregistration is very serious.

P. Conclusions/Second Design

The second design was considered (actually reconsidered) in depth because of the destructive effect of false alarms due to stars just below the threshold. As this effect is threshold independent, it cannot be overcome except by a great increase in the cost of repetition. Unfortunately this second system too suffers from a fatal flaw, namely the problem of misregistrations. We can see no way to overcome both of these difficulties, in a fully automated system, and provide interesting search rates, appropriately, faint.

VI. RESULTS TO DATE

Our results to date are summarized in Tables VIII, IX, and Fig. 30. Each Table provides the number of objects for which positional measurements have been made, the number of such observations, the number of nights we have actively searched, the number of square degrees covered, and the number of new minor planets found by us. The first Table provides a yearly summary, the second is by lunation. The Figure shows the upward trend in the sky coverage.

We have not found a new Earth-approaching asteroid by searching and this is statistically comparable to other searches of the past few years. It appears as if the estimate of 1000 Earth-approaching asteroids down to $B(1,0) = 18^m$ is incorrect.

A. Personnel

In addition to the constant encouragement and support of D. Batman, R. J. Bergemann, and V. A. Nedzel, several other members of the Space Surveillance Group have participated in refining our procedures. We wish to acknowledge the assistance of B. Lawrence, R. M. Martinson, G. J. Mayer, I. M. Poirier, K. M. Sommerer, S. A. Stansfield, and A. J. Wardrop. The actual asteroid observing work has also been a group effort. In particular, the contributions of D. E. Beatty, E. Chavez, R. L. Irelan, R. C. Ramsey, and L. Ward have been instrumental in making this work successful.

Many thanks to Lynne Perry - our exceptionally dedicated and highly skilled secretary - for her tireless persistence in deciphering the handwriting of L. G. Taff.

Table VIII

Asteroid Searches

Time Period	# Objects	# Observations	# Nights	# Sq. Deg.	# Discoveries
1979-1980 inclusive	45	96	5	200	2
1981	209	580	53	2785	33
1982	226	370	42	4610	27
1983 (to date)	71	163	33	8300	4

Table IX

Asteroid Searches By Lunation

Time Period	No. of Objects	No. of Observations	No. of Nights	No. of Sq. Deg.	Discoveries
1979-1980 inclusive	45	96	5	200	2
1981	209	580	53	2785	33
Jan.	22	58	3	200	0
Feb.	9	48	6	345	0
Mar.	8	24	6	300	0
Apr.	10	39	3	160	0
May	11	71	4	220	0
June	4	11	2	80	0
Aug.	37	133	8	550	8
Sept.	28	42	4	190	2
Oct.	46	86	5	275	14
Nov.	0	0	2	55	0
Dec.	34	68	10	410	9
1982	226	370	42	4612	27
Jan.	4	4	1	27	0
Feb.	38	58	5	275	8
Mar.	39	66	6	345	5
Apr.	20	57	6	330	2
May	43	50	6	275	2
Sept.	36	67	8	1390	1
Oct.	19	36	3	580	1
Nov.	76	10	3	580	3
Dec.	20	22	4	810	5

C-2

Table IX (Cont.d)

Asteroid Searches By Lunation

Time Period	No. of Objects	No. of Observations	No. of Nights	No. of Sq. Deg.	Discoveries
1983					
Jan.	25	48	4	930	3
Feb.	13	43	7	1860	1
Mar.	12	30	8	1740	0
Apr.	11	22	6	1680	0
May	10	20	8	2090	0

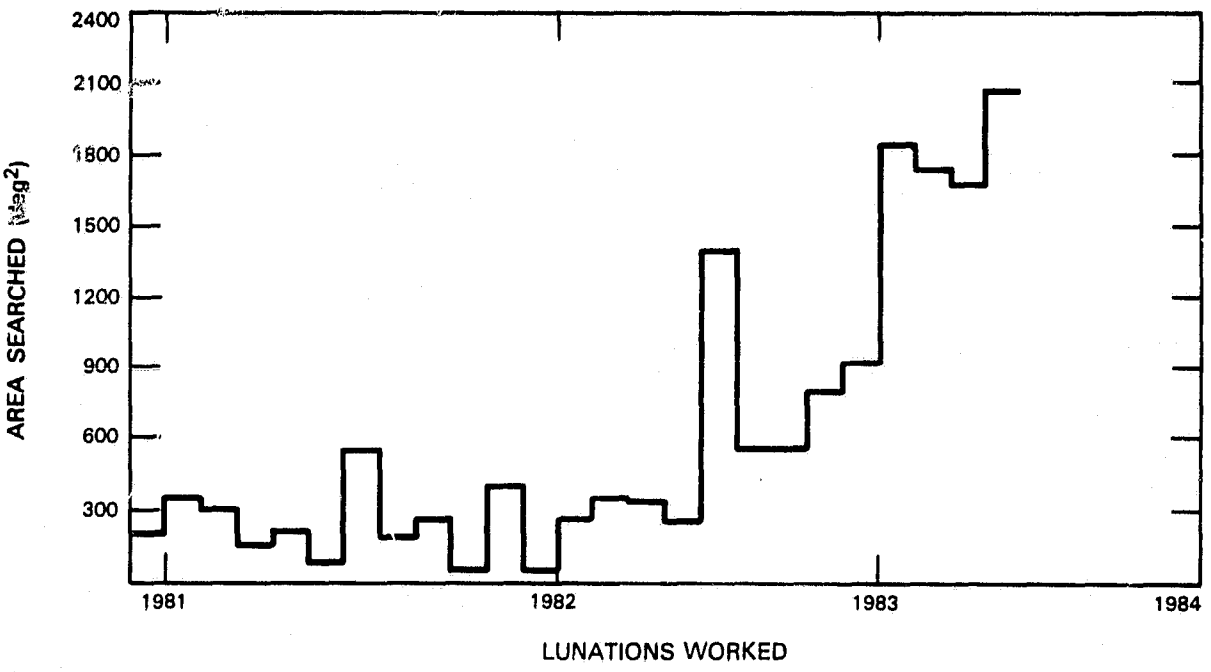

Figure 30. Sky coverage as a function of lunation.

References

Kostishack, D. F., Burke, B. E., and Mayer, G. J., Proc. SPIE 252, 44, 1980.

Kostishack, D. F., Gylfphe Jr., C. H., MacDonald, M. J., and Pong, N. G. S., Lincoln Laboratory Tech. Rep. 539, 1980.

Taff, L. G., Lincoln Laboratory Tech. Rep. 628, 1983a.

Taff, L. G., submitted to Icarus, 1983b.

Taff, L. G. and Hall, D. L., Cel. Mech. 16, 481, 1977.

Taff, L. G. and Hall, D. L., Cel. Mech. 21, 281, 1980.

Weber, R., Opt. Eng. 18, 82, 1979a.

Weber, R., Proc. SPIE 203, 6, 1979b.

Bibliography

The references listed above have already been supplied to NASA in sets of ten. Those listed below have either been referenced in our proposals or earlier Semi-Annual Status Reports. They are included here for completeness and have been supplied in sets of ten previously. I have not reiterated the Minor Planet Circulars publications.

Beatty, D. E., Sorvari, J. M. and Taff, L. G., Lincoln Laboratory Proj. Rep. ETS-53, 1980.

Sorvari, J. M., Lincoln Laboratory Proj. Rep. ETS-37, 1978.

Taff, L. G., Lincoln Laboratory Tech. Rep. 1980-24, 1980.

Taff, L. G., P.A.S.P. 93, 658, 1981.

Taff, L. G., Lincoln Laboratory Proj. Rep. ETS-61, 1982.

Taff, L. G., Lincoln Laboratory Proj. Rep. ETS-64, 1982.

Taff, L. G. and Poirier, I. M., Lincoln Laboratory Proj. Rep. ETS-30, 1978.

Taff, L. G. and Sorvari, J. M., Cel. Mech. 26, 423, 1982.